Effect of Reaction Furnace and Converter Temperatures on Performance of Sulfur Recovery Units (SRUs)

Hamid Reza Mahdipoor, Keyvan Khorsand, Reza Hayati, Hooman Javaherizadeh

Department of Process and Equipment Technology Development, Research Institute of Petroleum Industry, West Blvd. of Azadi Stadium, Tehran, Iran

mahdipoorhr@ripi.ir

***Abstract*-The modified Claus process is commonly used in oil refining and gas processing to recover sulfur and destroy contaminants formed in upstream processing. In oil refining, in addition to the typical modified Claus plant feed, i.e. H_2S and CO_2, NH_3, CS_2, and COS are also often present or formed. These contaminants pose a risk of poisoning the catalyst beds, as well decreasing the overall sulfur recovery. In this paper, effect of reaction furnace and converter temperatures on performance of SRUs is described. Then, the common ways for adjusting these important parameters are presented for a typical sulfur recovery unit. The achieved results can be useful for designing the new Claus sulfur recovery units.**

Keywords-Claus Process; Furnace and Converter Temperatures

I. INTRODUCTION

The Claus process continues to be the most widely used process for the conversion of H_2S to sulfur [1]. The task of Claus processes is to recover elemental sulfur from hydrogen sulfide and, more generally, from byproduct gases originating from physical and chemical gas and oil treatment units in refineries, natural gas processing, and gasification plants, to quote a few [2]. They consist of a thermal reaction furnace, a waste heat boiler, and a series of catalytic reactors (converters) and condensers (Figure 1). The reactions occurring in the furnace are numerous, and several authors have attempted to delineate the important ones [3-6]. The overall reaction characterizing the process is as follows [2]:

$$2H_2S + O_2 \Rightarrow S_2 + 2H_2O$$

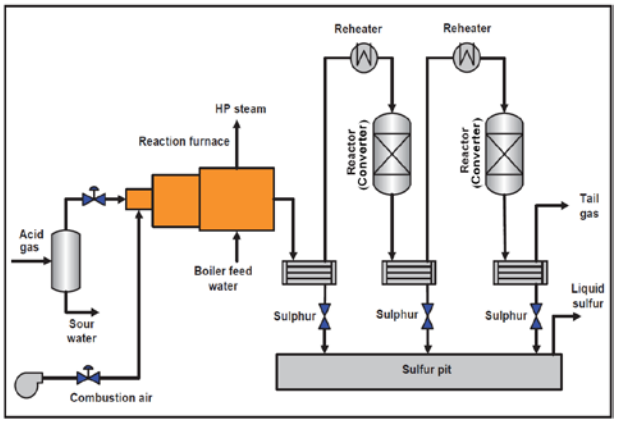

Fig. 1 The schematic shape of a typical Claus unit

In the first step or thermal stage, one-third of the H2S is completely oxidized to SO2 in the reaction furnace, locating at the front end of plant. A benefit that also occurs is the production of significant quantities of elemental sulfur (S2) from the thermal decomposition of H2S. In fact, the sulfur produced in the furnace is 50-60% of the total sulfur condensed in the plant. The main H2S oxidation reaction is [7],

$$H_2S + \frac{3}{2} O_2 \Rightarrow SO_2 + H_2O$$

The reaction furnace is followed by the waste heat boiler (WHB), where heat is recovered by cooling the furnace product gases [7]. In the second step that the catalytic stage, unreacted H2S is then combined with SO2, reacting via eq. 2, over an alumina catalyst to form elemental sulfur in fixed bed reactors by the following reaction [7,8],

$$2H_2S + SO_2 \Leftrightarrow \frac{3}{2} S_2 + 2H_2O$$

Since this reaction is exothermic, decreasing the temperature leads the equilibrium reaction toward right hand, i.e. more sulfur yields. On the other hand, low temperatures decrease the reaction rate. Therefore, an appropriate catalyst must be used to increase the reaction rate. However, high sulfur yields still necessitate a multistage process with inter-stage cooling and sulfur condensation [8].

Sulfur formed in each stage of the Claus plant is condensed and recovered to achieve maximum conversion in the catalytic reactors. The unrecovered sulfur, in elemental or combined form (H2S, COS, CS2), is combusted to SO2 in the tail gas incinerator which is then emitted to the atmosphere. Tail gas clean-up units are added sometimes prior to incineration to increase the sulfur recovery and minimize emissions [7].

One of the furnace functions is the destruction of any contaminants what may foul downstream equipments. In oil refinery operations, NH3 is formed as a byproduct what is then directed to the sulfur recovery facility for destruction [5]. Incomplete pyrolysis or combustion of NH3 in the furnace results in NH3 and NO carryover into the catalyst beds. Ammonia can form ammonium salts, which can plug or foul the catalyst beds, other equipments, or piping. Although the formation of SO3 occurs in the catalyst bed regardless of the presence of NO, the presence of NO in the beds acts as a catalyst for the conversion of SO2 to SO3, which in turn causes catalyst sulfation [9]. Of the primary causes of catalyst activity loss, catalyst sulfation is regarded as the most significant [10]. It is therefore critical to convert as much NH3 to N2, H2, and H2O as possible.

For ammonia destruction, an empirical rule of thumb in industry is that furnace temperature should be greater than 1200-1250 °C [5]. The furnace temperature must be below the temperature limitation of conventional refractories of 1600°C and above the minimum stable furnace temperature of 926°C

[11]. The reaction furnace temperature should not exceed 1380 °C in order not to exceed the maximum temperature limitations of the equipment materials [12].

In the Claus process, other sulfur compounds will be formed, such as carbon disulfide (CS2) and carbon oxysulfide (COS), and these compounds can often contribute from 20 to 50% of the pollutants in the tail-gas [13,14]. Furthermore, presence of O2 traces in the CS2-H2O mixture caused a decrease in the activity of alumina and titania catalysts due to sulfate formation [15]. Therefore, COS and CS2 should be hydrolyzed in the catalytic converter [16, 17], as shown below:

$$COS + H_2O \leftrightarrow H_2S + CO_2$$

$$CS_2 + 2H_2O \rightarrow 2H_2S + CO_2$$

The temperature of the first catalytic reactor is maintained at about 350°C to hydrolyze COS and CS2, while that of the subsequent reactors is just above the sulfur vapor dew point [18]. Transition metal oxides can be used to modify gamma-alumina to form a catalyst that is effective at temperatures higher than the dew point of sulfur [19-21]. However, thermodynamics provide a strong incentive to operate the catalytic converters at low temperature [22, 23] as a lower temperature should increase the exothermic reaction efficiency. Therefore, the temperature of the process gas at the inlet of the catalytic converters should be such that the effluent gas temperature is about 14-17°C higher than the expected outlet sulfur dew point and high enough for hydrolysis of COS and CS2 for the first catalytic converter only [24] (about 350°C).

In this paper, the temperature of reaction furnace of a typical Clause Sulfur Recovery Unit is adjusted to ensure suitable NH3 destruction. Moreover, the inlet temperatures of SRU converters are determined such that the proper conversion can be achievable without any processing problems. The process temperatures are important in designing the Claus sulfur recovery units.

II. SRU REACTION FURNACE

As mentioned before, since only one-third of H2S convert to SO2 in the reaction furnace, the unreacted H2S and inert gases consume the released energy from this exothermic reaction and the furnace reach to a thermal equilibrium. It decreases the temperature of reaction furnace. For this reason, a split-flow reaction furnace design (Figure 2) is applied to process the gas streams containing considerable amounts of ammonia. In this method, all the combustion air and all the ammonia containing sour gas are mixed with a portion of the acid gas stream and inserted to the first zone of the furnace and the remaining acid gas is then mixed with the products of the combustion from the first zone in zone 2 of the reaction furnace [25,26].

For illustrating the split-flow method, the Claus unit of a typical refinery is considered. The SRU feedstock consists of 74 Kmole/h acid gas from amine sweetening unit at 46°C and 1.3 bar, together with 38 Kmole/h sour gas from sour water treating unit at 90°C and 1.5 bar. The molar compositions of these streams are presented in Table The sour gas containing 275 Kg/h ammonia and therefore, the furnace temperature should increase, up to the ammonia destruction temperature. For this reason, a case study is performed in which the acid gas split into two zone. Figure 3 illustrates the achieved results. The horizontal axis indicates the ratio between the flow rate of acid gas entered to zone 1 and the flow rate of acid gas entered to zone 2. The vertical axis represents the changes of the first zone temperature.

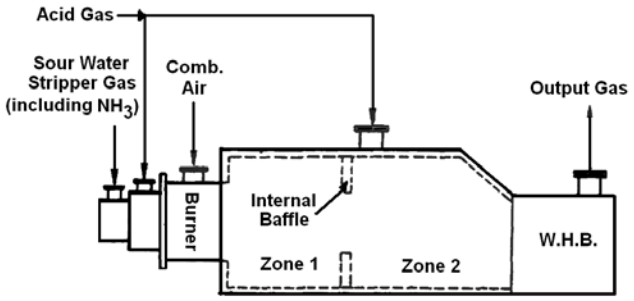

Fig. 2 A split-flow reaction furnace design

TABLE I THE COMPOSITION OF THE CLAUS UNIT OF FEEDSTOCK

Component	Mole Fraction	
	Acid Gas	Sour Gas
H_2S	91.6	24.3
H_2O	7.3	33.2
C_2H_6	1.1	0
NH_3	0	42.5

If combustible gases enter to the furnace first zone as their stoichiometric coefficients, the reaction furnace temperature will be maximized, for no excess gas or excess oxygen (excess air) is there. The maximum point of this curve is related to this condition. Before this point, the amounts of combustible gases (including H2S) are less than needed one-third of total H2S and therefore, temperature is decreased. Regarding to Figure 3, if the split-flow ratio was equal to 0.8, a temperature around 1350°C would be achievable for zone 1 of the reaction furnace. This temperature guaranties the complete destruction of NH3. If more expensive refractory with better resistance was applied, the furnace would be operate at higher temperatures by decreasing this ratio (see Figure 3).

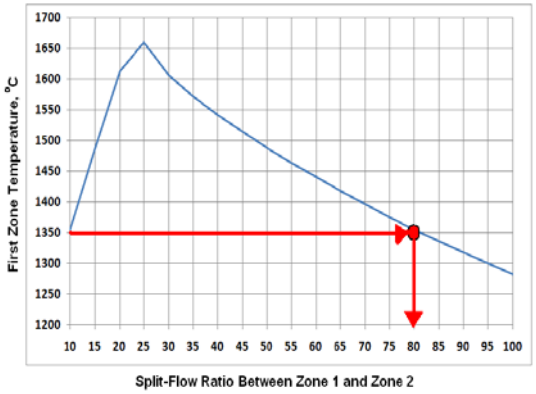

Fig. 3- A split-flow ratio between zone 1 and zone 2 vs. variations of zone 1 temperature

The operating problems related to the split-flow design including inadequate destruction of hydrocarbons and ammonia that might be contained in the bypassed portion of the acid gas and inadequate reaction of furnace residence time for thermal Claus sulfur conversion. The alternate way to overcome these problems is preheating the acid gas and combustion air and using high-intensity burners in the reaction furnace [11].

III. SRU REACTORS (CONVERTERS)

The temperature of the process gas at the inlet of the catalytic converters should be such that the effluent gas

temperature is about 14-17°C higher than the expected outlet sulfur dew point. For this purpose, the outlet streams of two converters in the above plant are investigated. Table Ⅱ presents pressure, temperature, and compositions of outlet streams of these converters. These data are achieved by the assumption of 265°C for temperature of the first converter inlet stream and 195°C for temperature of the second converter inlet stream.

TABLE Ⅱ THE OUTPUT CONDITIONS OF CLAUS CONVERTERS

	Converter 1	Converter 2
Pressure (bar)	1.1	1.05
Temperature (°C)	310	225
	Component (mass%)	
H_2S	2.8	0.8
H_2O	22.9	28.0
CO_2	0.6	0.7
SO_2	2.7	0.8
H_2	0.2	0.2
N_2	56.4	65.7
Sulfur	14.4	3.8

Figure 4 represents the variations of vapor phase fraction vs. outlet temperatures of two Claus reactors. According to this figure, dew point of the first converter outlet stream is equal to 253°C which is 57°C less than its assumed temperature from Table 2. With respect to criterion of 14-17°C, the temperature of 270°C seems to be appropriate for the outlet temperature of first converter. However, this temperature should be increased to ensure hydrolysis of COS and CS2 in the first reactor. Therefore, the assumption of 265°C is a good value for the temperature of the first converter inlet stream. Furthermore, dew point of second converter outlet stream is equal to 210°C which is 15°C less than its assumed temperature value from TableⅡ and takes the above criterion in the consideration.

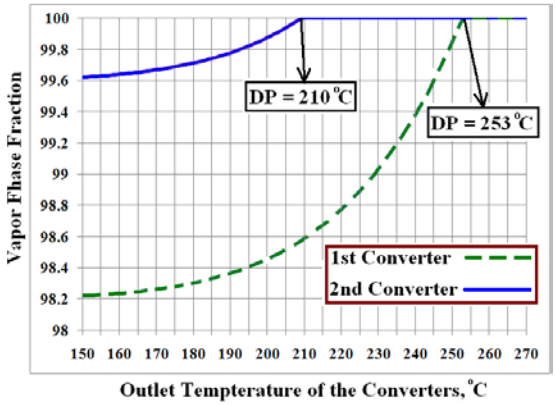

Fig. 4 The variations of vapor phase fraction vs. outlet temperatures of SRU reactors

IV. CONCLUSION

The modified Claus process was introduced as a commonly unit to recover sulfur and destroy contaminants formed in upstream processing. In these units, in addition to converting H2S to sulfur, other contaminants such as NH3, CS2, and COS must be eliminated. Rigorous adjustment of process temperatures is important to achieve this purpose. In this paper, the parameters that may affect adjusting the temperature of furnace and converters were investigated by means of analyzing a typical sulfur recovery unit. The achieved results illustrate a method which is useful for designing the new sulfur recovery units.

REFERENCES

[1] Zare Nezhad, B., An investigation on the most important influencing parameters regarding the selection of the proper catalysts for Claus SRU converters, *J. Ind. Eng. Chem.* 15 (2009) 143-147.

[2] Signor, S., Manenti, F., Grottoli, M. G., Fabbri, P., and Pierucci, S., Sulfur Recovery Units: Adaptive Simulation and Model Validation on an Industrial Plant, Ind. Eng. Chem. Res. 49 (2010) 5714-5724.

[3] Hawboldt, K. A.; Monnery, W. D.; Svrcek, W. Y. A Study on the Effect of Quench Design on the Quality of Experimental Data. Ind. Eng. Chem. Res., 38 (1999) 2260-2263.

[4] Hawboldt, K. A.; Monnery, W. D.; Svrcek, W. Y. New Experimental Data and Kinetic Rate Expression for H2S Cracking and Re-Association. Chem. Eng. Sci. 55 (1999) 957-966.

[5] Monnery, W. D., Hawboldt, K. A., Pollock, A. E. and Svrcek, W. Y., Ammonia Pyrolysis and Oxidation in the Claus Furnace, Ind. Eng. Chem. Res. 40 (2001) 144-151.

[6] Clark, P. D., Dowling, N. I., Huang, M., Chemistry of the Claus Front-End Reaction Furnace. Hydrocarbon Reactions and the Formation and Destruction of CS_2. Proceedings of the Brimstone Sulfur Recovery Symposium, Vail, CO, Sept (1997) 23-26.

[7] Nasato, L. V., Karan, K., Mehrotra, A. K., and Behie, L. A., Modeling Reaction Quench Times in the Waste Heat Boiler of a Claus Plant, *Ind. Eng. Chem. Res*. 33 (1994) 7-13.

[8] Elsner, M. P., Menge, M., Müller, C., Agar, D. W., The Claus process: teaching an old dog new tricks, *Catalysis Today* 79–80 (2003) 487-494.

[9] Garside, J. E.; Phillips, R. F. Pure and Applied Chemistry; Pittman and Sons Ltd.: London, 1962.

[10] Grancher, P. Advances in Claus Technology. Hydrocarbon Process. 1978, 57 (7), 155-160.

[11] Kohl, A., Nielsen, R. B., Gas Purification, 5th ed., Gulf Publishing Company, Houston, Texas, 1997.

[12] Sassi, M. and Gupta, A., K., Sulfur Recovery from Acid Gas Using the Claus Process and High Temperature Air Combustion (HiTAC) Technology, American Journal of Environmental Sciences 4 (2008) 502-511.

[13] Gens, T.A., Decrease in Carbonyl Sulfide in the Feed to Claus Converters by Shift Catalysts, Ind. Eng. Chem. Res. 33 (1994) 1654-1656.

[14] Huisman H.M., P. van der Berg, R. Mos, A.J. van Dillen, and J.W. Geus, Hydrolysis of Carbon Sulfides on Titania and Alumina Catalysts: The Influence of Water, Applied Catalysis A, 115 (1994) 157-172.

[15] Laperdrix, E., I. Justin, G. Costentin, 0. Saur, J.C. Lavalley, A. Aboulayt, J.L. Ray, and C. Nedez, Comparative Study of CS2 Hydrolysis Catalyzed by Alumina and Titania, Applied Catalysis B: Environment, 17 (1998) 167-173.

[16] Puchyr, D.M J., A.K Mehrotra, LA Behie, and N. Kalogerakis, Hydrodynamic and Kinetic Modeling of Circulating Fluidized Bed Reactors Applied to a Modified Claus Plant, Chem. Eng. Sci. 51 (1996) 5251-5262.

[17] Maadah, A.G. and R.N. Maddox, Predict Claus Product, Hydrocarbon Processing 57 (1978) 143-146.

[18] Burns, R.A., R.B Lippert, and R.K. Kerr, Choose Catalyst Objectively, Hydrocarbon Processing, 53 (1974) 181-186.

[19] George, Z.M., Effect of Catalyst Basicity for COS, SO_2 and COS Hydrolysis Reactions, J. catalysis, 35 (1974) 218-224.

[20] Terorde, R.J.A.M., PJ. van den Brink, L.M. Visser, A.J. van Dillen, and G.W. Geuss, Selective Oxidation of Hydrogen Sulfide to Elemental Sulfur Using Iron Oxide Catalysts on Various Supports, Catalysis Today 17 (1993) 217-224.

[21] Berben, P.H., Ph.D. Thesis, University of Utrecht, The Netherlands, 1992.

[22] Ledoux, M.J., P.H. Cuong, N. Keller, J.B. Nougayrede, S. Savin-Poncet, and J. Bousquet, Selective Oxidation of H_2S in Claus Tail-Gas over SiC Supported NiS_2 Catalyst, Catalysis Today 61 (2000) 157-163.

[23] Kerr, K.R., Energy Processing Canada, pp 28-35, July-August 1976.

[24] Gas Processors Suppliers Association (GPSA). Engineering Data Book; GPSA Tulsa, 1987; Chapte.

[25] Wiley, S., Off-gas aids Claus operations," Hydro. Process. 59 (1980) 127-129.

[26] Chute, A. E., Tailor sulfur plants to unusual conditions, Hydro. Process. 56 (1977) 119-124.

Rheological Evaluation of Surfactants with Potential Application as Divergent Agents

Fernanda C. Lechuga[1], Claudia R. E. Mansur[1], Maria Carmem M. Bezerra[2], Luiz Cesar F. Barbosa[2], Elizabete F. Lucas[1]

[1]Federal University of Rio de Janeiro – Institute of Macromolecules – Laboratory of Macromolecules and Colloids in Petroleum Industry - Av. Horácio Macedo, 2030 – Ilha do Fundão, 21941-598, Rio de Janeiro, RJ, Brazil

[2]Petrobras Research Center/CENPES – Q. 7 – Cidade Universitária, 21949-900, Ilha do Fundão, Rio de Janeiro, RJ, Brazil

[1]celias@ima.ufrj.br; [1]elucas@ima.ufrj.br; [2]maria.cmb@petrobras.com.br; [2]lcesar@petrobras.com.br

***Abstract*-Viscoelastic surfactants are very useful in various oilfield operations, such as enhancing oil recovery and hydraulic fracturing and acidification. Because of the permeability differences in the rock reservoir, a large part of the fluid injected can migrate to undesired regions. Therefore, viscous fluids are used to modify the permeability of certain regions of the rock formation. The products added to the fluids that provide this characteristic are called divergent agents. There are a large number of commercial products that can be used for this purpose, but the fluids prepared with them must have special properties. Therefore, it is essential to evaluate these products in advance. This work examines the chemical structure and physic-chemical properties of commercial surfactants to identify those with potential application as divergent agents. To do this, the rheological behaviour of the commercial formulations was tested considering temperature and pH conditions typical of reservoirs.**

Keywords-Divergent Agents; Surfactants; Rheology; Surface Tension; FTIR

I. INTRODUCTION

Extraction of petroleum requires the use of various processes. Many of these involve injection of fluids in the porous formations where the oil is found, for example acidification, hydraulic fracturing and scale inhibition.

Hydrocarbon reservoirs are constituted of layers with different permeabilities, due to natural phenomena or invasion of mud. Therefore, when a fluid is injected into the rock formation, it will preferentially migrate to the more permeable zones around the bore hole, leaving the zones that mostly need of treatment intact. It is thus necessary to use a technique that induces the process fluid to diverge to zones with low permeability, allowing a more uniform fluid distribution among the various zones. This is achieved by temporarily obstructing the more permeable zones by using a fluid containing additives called divergent agents, to permit treatment of less permeable zones [1-11].

In the majority of applications of this technique, an initially low-viscosity polymer solution is injected in the reservoir. Upon reaching the target zone, the solution becomes more viscous, reducing the permeability of that part of the reservoir. This can be achieved by the transformation of the solution into a gel, either spontaneously or by chemical induction [7].

These solutions often present non-Newtonian behaviour, i.e., their viscosity depends on the flow rate (more specifically, the shear rate). The most common behaviour presented by these polymer solutions is pseudo-plastic, in which the viscosity declines with an increase in the shear rate. In certain cases the solution has low viscosity when flowing through pipes and during injection toward the rock formation's pores. Then the solution migrates radially through the formation, the flow rate and associated shear rate decline and the solution's viscosity increases. In many oilfield operations, this increased viscosity with reduced flow rate creates a gel that is sufficiently strong to have the desired divergent effect [11].

Many reticulation agents have been used. They can be classified as the inorganic (for example, chrome, zirconium, aluminium and borate) or the organic (phenol/formaldehyde, aldehydes or acetates, polyamides) [7,12,13].

The reservoir conditions are relatively aggressive to certain injected substances due to variations in temperature, salinity, pH and other observable factors.

Currently there are few gels that can be used under adverse conditions. The polymers used in these gels include polyacrylamides with low molar mass, natural polymers and special polymers developed to tolerate these conditions. Metallic reticulation agents can be used to produce gels with anionic polymers. This is achieved through the formation of ionic bonds between multivalent captions and negative sites of the polymer. The gels produced through metallic reticulation agents typically are less thermally stable. Organic reticulation involves the formation of covalent bonds between functional groups of the polymer and the reticulation agent, connecting two or more polymer chains. To obtain thermally stable gels, it is necessary to start with thermally stable polymers [7].

The use of viscoelastic surfactants in aqueous fluid systems has also been reported. The surfactants being used are mixed ionic or amphoteric, such as dihydroxyl alkyl glycinate, alkyl betaine, alkyl amidopropyl betaine and e alkylamino mono- or di- propionate, derived from certain waxes, fats and oils. The surfactant is used together with inorganic salts, organic acids and organic acid salts or combinations of these additives [14].

This paper reports the results of studies of the rheological behavior of aqueous formulations of a series of surfactants, in comparison with two commercial divergent agent formulations.

II. EXPERIMENTAL

A. Surfactant Systems

The surfactant systems used in this work were donated by Rhodia do Brasil, SP-Brazil described below.

- System S1

- Mixture of butyl ether hydroxypropyl sultaine and 2-ethyl-hexyl ether hydroxypropyl sultaine – 50% and 43%

- NaCl – 7.16%

- Water

• System S2

- Cocamidopropyl hydroxyl sultaine – 49.57%

- Color gardner – 0.2%

- NaCl – 6.65%

- Water

• System S3

- Dihydroxyethyl tallow glycinate (betaine) – 41.8%

- NaCl – 5.3%

- Water

• System S4

- Sodium lauriminodipropionate (28 to 31%)

- Water (69 a 72%)

- pH: 6-7

• System S5

- Sodium alkyliminopropionate (41 to 44%)

- Methanol (6-8%)

- Water (48 to 51%)

- pH: 10-11

• System S6

- Ethoxylated alkyl sodium sulphate (25-28%)

- Water (72-75%)

- Dioxane (<0.09%)

- Ethylene oxide (<0.001%)

• System S7

- Sodium alkyl ether sulphate (69-71%)

- Water (29-31%)

- Dioxane (<0.009%)

- Ethylene oxide (<0.001%)

The commercial divergent agent formulations utilized (system C1 and system C2), as well as the procedure of preparing each of the fluids, are reported below.

• System C1

System C1 is supplied ready to use by the manufacturer. We only added ammonium chloride salt (NH_4Cl) to increase its viscosity. The base composition is the following:

- Aliphatic amine derivative (base surfactant) – 60-100%;

- 2-propanol – 10-30% p/v;

- 1,2-propanediol – 10-30% p/v;

- Water – 5-10% v/v.

Before adding the salt to system C1, we pipette two 5-mL aliquots into aluminium capsules, previously weighed, to calculate the concentration of the base surfactant in the formulation. The aliquots were placed in a circulating air chamber at 100 ^oC and left there until the aluminium capsules reached constant weight. The base surfactant concentration determined by this method was 61% wt/v.

To add the salt to the system, we first dissolved NH_4Cl in water at a concentration of 4% wt/v. The final formulation was prepared by slowly adding 25 mL of the base formulation to the brine, under mechanical stirring at 1000 rpm. After the addition was completed, the stirring speed was increased to 2000 rpm for about 30 minutes.

• System C2

System C2 is composed of an amphoteric surfactant (base surfactant), to which other components are added according to the manufacturer's orientation.

The ammonium chloride was added in distilled deionised water and stirred with a glass rod until completely dissolved. Then KOH was added until it was completely dissolved as well as the base surfactant. This mixture was homogenized using a mechanical stirrer at 2000 rpm for 20 minutes. Finally, the BF-7 LB compound was added until a gel formed, and this mixture was stirred for an additional 30 minutes at 2000 rpm. The final composition of system C2 was as follows:

- Industrial water – 4% v/v;
- Ammonium chloride – 4% wt/v;
- KOH – 0.5% wt/v;
- Amphoteric surfactant (base surfactant) – 3% wt/v;
- BF-7LB – 0.8%v/v

B. Chemical Characterization of the Base Surfactants

The structure of the base surfactants was characterized by qualitative analyses in a Perkin Elmer 1720x Fourier transform infrared (FT-IR) spectrometer, controlled by a DEC 320 sx station computer, with an IR data manager, also made by Perkin Elmer. We used the capillary film method, in which the samples are spread over a KBr cell and the film formed is covered with another KBr cell. All the analyses were performed using resolution of 2 cm^{-1}, 20 scans and a wavelength range of 4000-400 cm^{-1}.

The systems C1 and C2 were also analysed by nuclear magnetic resonance (NMR) in a Varian Mercury 300 spectrometer, at the following experimental settings: observed nucleus - ^1H; frequency - 300.067 MHz; concentration - ~ 1% wt/v; internal reference – tetramethylsilane (TMS).

Finally, we evaporated the samples in a vacuum chamber to eliminate solvents and other possibly volatile constituents. This treatment does not eliminate the salts present in the samples.

C. Analysis of the Surface Tension of the Surfactant Systems

We measured the surface tension of the solutions in triplicate, at 25^oC, in a Krüss K10ST digital tensiometer. For each sample, we plotted a graph of the average surface tension (in mNm^{-1}) against the logarithm of the concentration (in %wt/v). We then used this graph to determine the critical micelle concentration (CMC).

D. Rheological Evaluation of the Surfactant Systems

We performed the rheological evaluation in a Haake RS600 rheometer.

Depending on the viscosity value, it used coaxial cylinders (Z20 and DG41) or a cone/plate accessory, with cone diameters of 35 and 60 mm and an angle of 1º. We analysed the systems at temperatures of 25 and 5 oC and pH interval of 1 to 14. We carried out these analyses in function of the increase and decrease of the shear rate. Since the systems are intended for an application where the fluid will be submitted to a certain shear rate and then a lower one, we recorded the viscosity values as the shear rate was being reduced.

III. RESULTS AND DISCUSSION

A. Chemical characterization of the Base Surfactants

The probable structures of the base surfactants of the various systems, given by the manufacturers and confirmed by the spectrometric analyses, are listed in Table Ⅰ. By the chemical structures of surfactants and data of surface tensions and CMC, we expected to establish some kind of relationship with the rheological performance of the systems.

TABLE Ⅰ PROBABLE STRUCTURES OF THE SYSTEMS BASE

System	Classification of the manufacturer	Probable structures of the base surfactants
S1	Mixed ionic surfactant: mixture of butyl ether hydroxypropyl sultaine and 2-ethyl-hexyl ether hydroxypropyl sultaine	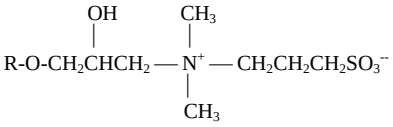
S2	Mixed ionic surfactant: Cocamidopropyl hydroxyl sultaine	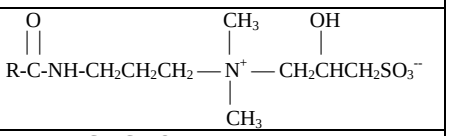
S3	Mixed ionic surfactant: Dihydroxyethyl tallow glycinate (betaine)	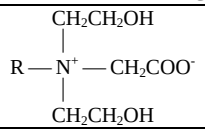
S4	Amphoteric surfactant: Sodium laurimino dipropionate	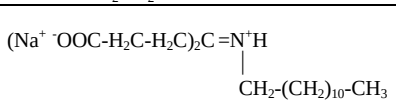
S5	Amphoteric surfactant: Sodium alkylimino propionate	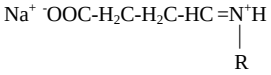
S6	Ethoxylated alkyl sodium sulphate	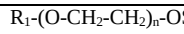
S7	Sodium alkyl ether sulphate	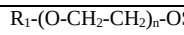
C1	Amphoteric surfactant	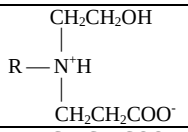
C2	Amphoteric surfactant	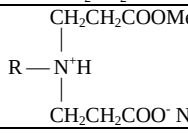

B. Measurement of the Surface Tension and Critical Micelle Concentration of the Surfactants

Table Ⅱ presents the surface tension values of the aqueous solutions containing each base surfactant, at concentrations of 10-4 and 0.3%v/v, and the CMC values. Systems S1 and S7 were not analysed because these formulations presented phase separation when diluted in water.

TABLE Ⅱ
SURFACE TENSION AND CMC RESULTS OF THE SYSTEMS

System	Initial surface tension (mNm^{-1}) [(a)]	Final surface tension (mNm^{-1}) [(b)]	CMC (% v/v)
S1	-	-	-
S2	70	32	10^{-2}
S3	65	36	10^{-2}
S4	69	33	10^{-2}
S5	71	39	3×10^{-1}
S6	65	33	8×10^{-2}
S7	-	-	-
C1	56	35	2×10^{-3}
C2	69	30	10^{-2}

[(a)] Initial surface tension obtained at a concentration of 10^{-4} %v/v

[(b)] Final surface tension obtained at a concentration of 0.3 %v/v

Except for system C1, all the others behaved similarly at a base surfactant concentration of 10-4 %v/v, that is, the surface tensions of the solutions were at ~70 mNm^{-1}. At concentrations above the CMC these values declined to around 35 mNm^{-1}, and the CMC values were above 10-2 %v/v. On the other hand, system C1, at a low base surfactant concentration (10-4 %v/v), already reduced the surface tension of the water to nearly 56 mNm^{-1}, and also had the lowest CMC (2 x 10-3 %v/v). Only the surface tension values at concentrations above the CMC were similar to those found for the other solutions of the products tested.

Because system C1 presented the lowest surface tension at low concentration and the smallest CMC *Except for system C1*, all the others behaved similarly at a base surfactant concentration of 10-4 %v/v, that is, the surface tensions of the solutions were at ~70 mNm^{-1}. At concentrations above the CMC these values declined to around 35 mNm^{-1}, and the CMC values were above 10-2 %v/v. On the other hand, system C1, at a low base surfactant concentration (10-4 %v/v), already reduced the surface tension of the water to nearly 56 mNm^{-1}, and also had the lowest CMC (2 x 10-3 %v/v). Only the surface tension values at concentrations above the CMC were similar to those found for the other solutions of the products tested. Besides performing the best in the rheological analyses (see latter), we performed analyses of the surface tension versus concentration, varying the pH of this system through the addition of hydrochloric acid or sodium hydroxide. The results are shown in Table Ⅲ.

TABLE III SURFACE TENSION AND CMC RESULTS OF SYSTEMS C1 WITH DIFFERENT PH VALUES

pH	Initial surface tension (mNm^{-1}) [(a)]	Final surface tension (mNm^{-1}) [(b)]	CMC (% v/v)
2	70	34	3×10^{-3}
6	56	35	2×10^{-3}
13	55	34	1.5×10^{-3}

[(a)] Initial surface tension obtained at a concentration of 10^{-4} %v/v

[(b)] Final surface tension obtained at a concentration of 0.3 %v/v

At a surfactant concentration of 0.3%, the surface tension values were similar in all three pH conditions tested. This result is coherent with the fact that the same structure occupies the interface in all three cases, and above the CMC the interface is totally (or nearly all) occupied by the surfactant species, that is, under the three conditions the structure is the same, with the same concentration at the interface, so the surface tension values are equal. However, at a concentration of 0.0001 % the surface tensions were quite different for pH 2. This behaviour is related to the fact that the amphoteric surfactant assumes a cationic form at low pH. In the specific case of the surfactant studied, the N+ group, which interacts more strongly with water than the –COO- and –O- groups do [15], makes the surfactant more hydrophilic, and at a given concentration, fewer species migrate to the interface, resulting in higher surface tension, that is, a lower value but near that of pure water. This behavior could also be observed with respect to the CMC values, because the cationic species, which is more soluble in water, has a higher CMC than the zwitterionic or anionic species do.

C. Rheological Evaluation of the Surfactant Systems

1) Tests in Function of the Shear Rate and Temperature:

According to the literature [7], formulations considered good for use as divergent fluids must possess, among other aspects, viscosity values between 10 and 20 cP at 50°C and shear rates around $70s^{-1}$. Besides this, when the shear rate falls to $10s^{-1}$, the formulation's viscosity cannot vary drastically (up to ~ 60 cP), and the desired behavior of the fluid should be moderately pseudo-plastic.

he tests of viscosity in function of shear rate were running at two temperatures to obtain two curves for each condition: tests with increasing and decreasing shear rates. In general, the curves obtained during the tests with rising shear rate coincided with those obtained during the falling shear rate tests. Figure 1 shows the curves obtained for system S5 as an example of the pseudo-plastic character and the differences observed as a function of the cycle measured (increasing or decreasing shear rate) for this system. Table 4 compiles all the results: viscosity values at two temperatures (25 and 50ºC) and two shear rates (70 and 10 s^{-1}). These values were taken from the curves of the viscosity in function of shear rate described during the falling rate tests. System S2 formed a thick film during the analysis at 50º C, and for this, its results are omitted from Table Ⅳ.

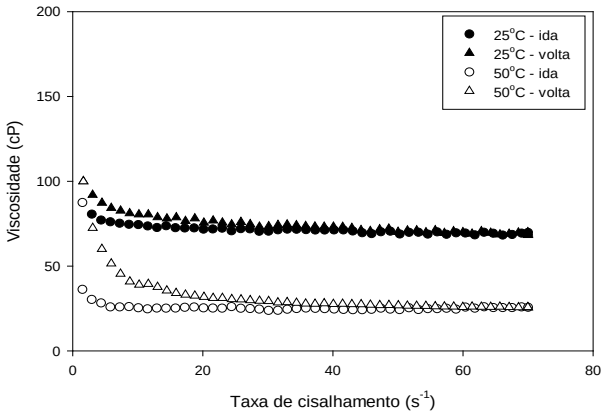

Fig. 1 Viscosity curves as a function of shear rate of system S5, at temperatures of 25 and 50°C

TABLE IV VISCOSITY RESULTS OF OBTAINED IN TESTS AT VARYING SHEAR RATES, AT 25, 50 AND 70 °C

System	Viscosity (cP)			
	25 ºC		50 ºC	
	70 s^{-1}	10 s^{-1}	70 s^{-1}	10 s^{-1}
S1	10	12	3	5
S2	90	90	**	**
S3*	50	114	5	9
S4	28	30	18	44
S5*	70	80	25	39
S6	24	25	26	200
S7	1,670	5,100	1,700	7,200
C1	70	335	65	130
C2	10	830	10	10

*Sample diluted in water in a proportion of 1:10 due to the gel form, which hampered viscosity measurement.

**The system was not measured at this temperature due to evaporation, evidenced by the formation of a film on the sample's surface.

The formulations of systems S3 and S5 supplied by the manufacturer showed high viscosity, with various bubbles trapped inside the gel formed. For this reason, we diluted these formulations in water in a proportion of 1:10 before performing the viscosity measurements.

As expected, the viscosity of all the systems fell with the increase in temperature, at both shear rates, with the exception of systems S6 and S7, which have an ethoxylated structure. This behavior is due to the reduction of their interactions with water as increasing temperature, until complete phase separation at a temperature above 50ºC.

In general, the systems showed pseudo-plastic behavior at the two temperatures tested, and the viscosity values were higher at lower shear rates. Since the main temperature of interest for application of divergent fluids is 50ºC, systems S2 and C2 could be eliminated because they do not have the required pseudo-plastic behavior at this temperature.

With respect to the ideal viscosity values at 50ºC, system S1 was much less viscous than desired. In an attempt to raise these values, we added NH_4Cl at a concentration of 4%wt/v to this system, but there was no change in viscosity.

Therefore, all the systems had the desired behaviour except for S1, S2 and C2, suggesting that the desired viscosities can be achieved just with adjustment of the concentration.

Because of the importance of knowledge of the behaviour of divergent fluid systems at the varied pH that can be found under oilfield conditions, we evaluated all the systems at different pH values, at a temperature of 25ºC, even those that did not present the desired pseudo-plastic behaviour. We chose this temperature for the initial tests because it allows easier measurement. Table Ⅴ shows the viscosity results at shear rates of 70 and 10 s^{-1}.

TABLE V VISCOSITY RESULTS OBTAINED IN TESTS WITH VARYING SHEAR RATES AT25 ºC, UNDER DIFFERENT PH CONDITIONS

System	Viscosity at 25 ºC (cP)						
	70 s^{-1}						
	2	**4**	**6**	**8**	**10**	**12**	**13**
S1	-	10	10	**	**	11	-
S2	-	89	91	90	95	-	-
S3*	-	48	50	-	-	-	-
S4	-	-	27	33	-	-	-
S5*	-	3	**	**	70	-	-
S6	-	38	**	24	**	**	315
S7	-	-	-	-	-	-	-
C1	70	70	70	70	70	70	70
C2	-	-	-	10	-	-	-
	10 s^{-1}						
S1	2	4	6	8	10	12	13
S2	-	12	12	**	**	13	-
S3*	-	85	91	90	96	-	-
S4	-	110	114	-	-	-	-
S5*	-	-	47	35	-	-	-
S6	-	3	**	**	80	-	-
S7	-	34	**	25	**	**	411
C1	-	-	-	-	-	-	-
C2	332	332	335	330	328	326	325
S1	-	-	-	830	-	-	-

* Sample diluted in water in a proportion of 1:10 due to the gel form, which hampered viscosity measurement.

** Analyses not performed

(-) Viscosity values not determined due to limitations of the technique or inadequacy of the formulations.

The viscosity values in boldface refer to those of the original formulation without the addition of hydrochloric acid or potassium hydroxide

Among the formulations that maintained their viscosity values in the pH range tested were S1, S6, and C1. System S1 had already been eliminated because of its very low viscosity values. System S6 resisted the pH variations, but there were significant viscosity changes at extreme pH values. The other systems presented phase separation with the pH variation or their viscosity values fell outside the detection range of the device.

Therefore, systems S6 and C1 were indicated for further testing at 50ºC, under the same pH conditions tested previously. However, we only tested system C1. That is because system S6, at 50 ºC and pH 8 (Table 4) did not show the desired pseudo-plastic behaviour (viscosities of 26 and 200 cP, respectively at 70 and 10 s^{-1}).

System C1 maintained its resistance to pH even at a temperature of 50 ºC, and showed viscosities of about 1,700 and 7,200 cP, respectively, for shear rates at 70 and 10 s^{-1}.

We performed other rheological tests of system C1 to verify its stability over time. For this purpose we chose shear rates at 10, 70, and 500 s^{-1} for the tests in function of time (30 minutes). No significant thyrotrophic behaviour was observed, meaning this system maintained the viscosity shown in Table 4 even after applying shear for 30 minutes.

2) Viscoelasticity Tests

We only performed viscoelasticity tests on system C1 since it was the only one that presenting viscosity values in the desired range, as well as having good resistance to pH variation. The first tests were carried out at a frequency of 1Hz, with variation of the amplitude. Figure 2 shows a region of linear viscoelasticity, that is, the region where the material's viscoelastic structure remains intact (up to a stress of 1 Pa). Besides this, it can be seen that the elastic component is much greater than the viscous component, which is expected of a gel.

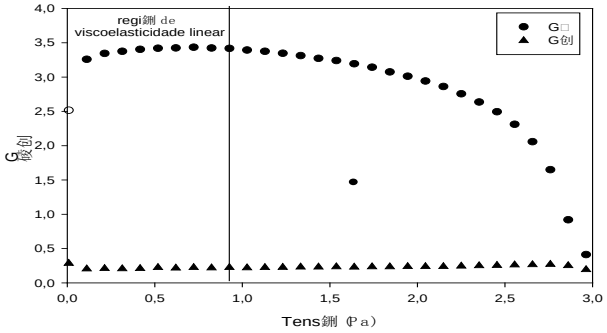

Fig. 2 G´ and G´´ curves in function of stress applied to system C1. Temperature: 25 ºC

From these results, we performed a creep-recovery test, which provides information on the material's stability and determines the ηo (viscosity of the sample with shear approaching zero). This test is carried out by applying a constant stress to the material for a determined time interval, where this stress is chosen in the region of linear viscoelasticity. After this interval, the stress is removed (stress = zero) and the material's recovery from deformation is observed. The tests were carried out applying stresses of 0.1 and 0.3 Pa for thirty seconds, and material recovery times of ten and thirty minutes, respectively. The results presented in Figure 3 show that the values of ηo calculated for the stresses of 0.1 and 0.3 Pa were equal at 46,270 and 44,140 cP, respectively, which were mutually concordant. Besides this, we observed the recovery time from deformation of system C1, at different stresses. When a stress of 0.1 Pa was applied for thirty seconds, there was almost total recovery after about ten minutes, while under stress of 0.3 Pa for the same thirty seconds the recovery took about thirty minutes. These results evidence the recovery capacity of this fluid under the conditions tested.

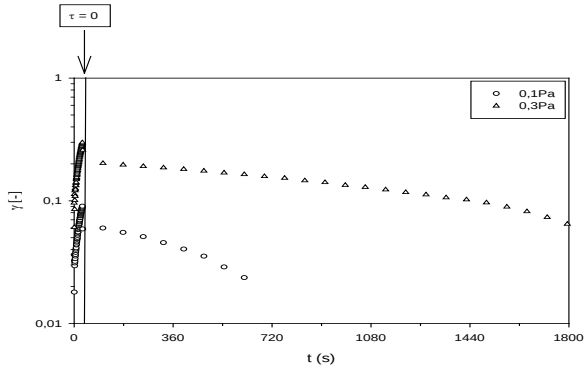

Fig. 3 Creep-recovery for system C1 at 25ºC

V. CONCLUSIONS

Among the surfactants tested, formulation C1 had the smallest CMC (4 x 10-3 %v/v) and greatest capacity to reduce surface tension (56 mNm^{-1}), at a low concentration (10^{-4} %v/v). Formulations C2, S3 and S2 showed mutually similar values for both CMC (~ 10^{-2} %v/v) and reduction of surface tension (~ 68 mNm^{-1}), at low concentrations.

Formulation S1 also showed good resistance to variations of pH and temperature, but it had low viscosity values. The formulations sensitive to increased temperature were C2, S2, S5 and S6, which evaporated at temperatures of 70, 80, 50 and 50 ºC, respectively. The formulations sensitive to variations of pH were C2, S2, S3, and S4, which showed phase separation at pH values below 5, above 11, above 6 and below 4, respectively.

The variation of pH did not significantly influence the physico-chemical properties of formulation C1. The CMC remained practically constant throughout the pH range tested and the surface tension reduction power was only impaired at low pH values (=2). This formulation also performed best regarding resistance to temperature and pH. This behavior can be related to the amphoteric structure of the base surfactant contained in this formulation. Besides this, it has high viscosity at small shear rates, with viscosity falling as the shear rate increases. Creep-recovery tests also demonstrated the recovery from deformation capacity of this formulation under the conditions analyzed probably associated with the physico-chemical properties of this formulation.

ACKNOWLEDGMENT

We thank the Rhodia do Brasil for donating the surfactants and the National Scientific and Technological Research Council (CNPq), the Office to Improve University Research (CAPES) and the Rio de Janeiro State Research Support Foundation (FAPERJ) for financial support.

REFERENCES

[1] L. L. Schramm, S. M. Kutay, R. J. Mikula, V. A. Munoz. “The morphology of non-equilibrium foam and gelled foam lamellae in porous media”, *J. Petrol. Sci. Eng.*, vol.23, pp. 117-132, 1999.

[2] A. Moradi-Araghi. “A review of thermally stable gels for fluid diversion in petroleum production”, *J. Petrol. Sci. Eng.*, vol.26, pp. 1-10, 2000.

[3] D. L. Purvis, D. D. Cramer, D. D. Smith, D. L. Walton. “Diversion treatment method”, US Patent 6 367 548, 2002.

[4] S. Siddiqui, S. Talabani, J. Yang, S. T. Saleh, M. R. Islam. “An experimental investigation of the diversion characteristics of foam in Berea sandstone cores of contrasting permeabilities”. *J. Petrol. Sci. Eng.*, vol. 37, pp. 51-67, 2000.

[5] S.Y. Hu, L. H. Zhang, H. J. YU. “Development and prospect of the profile control/water shutoff technology in reservoir high-capacity channels”. *Drilling & Production Technology*, vol. 29, 2006.

[6] S. Ma, M. Dong, Z. Li, E. Shirif. “Evaluation of the effectiveness of chemical flooding using heterogeneous sandpack flood test”. *J. Petrol. Sci. Eng.* vol. 55, pp. 294-300, 2007.

[7] R. Stalker, G. M. Graham, D. Oliphant, M. Smillie. “Potential application of viscosified treatments for improved bullhead scale inhibitor placement in long horizontal wells – a theoretical and laboratory examination”. *Society of Petroleum Engineers* 87439, 1-16, 2003.

[8] P. Albonico, T. P. Lockhart. “Divalent ion-resistant polymer gels for high temperature applications: Syneresis inhibiting additives”. Paper SPE 25220, presented at the 1993 SPE International Symposium on Oilfield Chemistry, New Orleans, LA, March 2–5, 1993.

[9] H. L. Hsieh, A. Moradi-Araghi, G. A. Stahl, I. J. Westerman. “Water-soluble polymers for hostile environment oil recovery applications”. *Makromol. Chem., Symp*., vol.64, pp. 121-124, 1992.

[10] R. D. Hutchins, H. T. Dovan, B. B. Sandiford. “Field applications of high temperature organic gels for water control”. Paper SPE/DOE 35444, presented at the 10th SPE/DOE Improved Oil Recovery Symposium, Tulsa, OK, April 21–24, 1996.

[11] Y. Liu, B. Bai, Y. Wang. “Applied technologies and prospects of conformance control treatments in China”. *Oil & Gas Science and Technology*, vol. 65, pp. 859-878, 2010.

[12] D. M. Chang. “Binding of free calcium íons in aqueous solution using chelating agents, phosphates and poly (acrylic acid)”. *J. Amer. Chem. Society*, vol. 60, pp. 618-622, 1983.

[13] S. Vossoughi. “Profile modification using in situ gelation technology - a review”. *J. Petrol. Sci. Eng.* vol. 26, pp. 199-209, 2000.

[14] M. S. Dahanayake, J. Yang, J. H. Y. Niu, P. J. Derian, D. Dino, R. Li. “Fluido contendo tensoativo viscoelástico e método para uso do mesmo” PI 9810023-8 A, 1998.

[15] J. T. Davies. “A quantitative kinetic theory of emulsion type I. Physical chemistry of the emulsifying agent”. Proceedings of the 2nd International Congress on Surface Activity; Edited by JH Schulman. New York, Academic Press, 426, 1957.

Preparation and Properties of Paraffin/Polyurethane Foams Composite with Flame Retardant as Thermal Energy Storage Materials

Liang Zhao[a], Gang Wang, Xiangchen Fang, Jianfeng Sun, Chunyan Yang

Fushun Research Institute of Petroleum and Petrochemicals, SINOPEC, Fushun, 113001, China

[a]zhliang2003@163.com

***Abstract*-Thermal energy storage plays an important role in energy conservation, and can be applied in many areas. Paraffin/polyurethane foams composite with flame retardant as thermal energy storage materials were prepared by absorbing paraffin in honeycomb structure of polyurethane rigid foams. These composites provide a new energy saving materials, which can be used for building heating/cooling systems, and the composites can also enhance the thermal comfort for residents. In the composites, paraffin was used as the phase change material (PCM), polyurethane (PU) rigid foams acting as the supporting material, or as nano-structured calcium carbonate (nano-CC) and red phosphorus (RP) acting as the flame retardant. The thermal properties, such as phase change temperature and latent heat, were investigated by a differential scanning calorimeter (DSC). Chemical structure, micro-structure and flame retardant properties of paraffin/ polyurethane foams composite were determined by FT-IR, SEM and limited oxygen index (LOI) tester, respectively. The SEM results showed that paraffin was well dispersed in honeycomb structure of polyurethane rigid foams. The DSC results indicated that the composites melt at 80.3℃ with a latent heat of 25.8kJ/kg when the mass percentage of paraffin in the composites was 16.7%. The LOI results showed that nano-CC and RP decreased the flammability of the composites.**

Keywords-Polyurethane Foams; Paraffin; Phase Change Materials; Flame Retardant; Thermal Energy Storage

I. INTRODUCTION

Today's storage problems and costly energy resources have become the primary force driving intensive development of phase change materials (PCMs) [1-6]. In latent heat storage system, thermal energy is stored in PCMs during a melting process while it is recovered during a freezing process. PCMs have received attention for various applications in solar heating systems [7-9], and building energy conservation [10-12]. Polyurethane rigid foams have been widely used for thermal insulation as the ultimate energy savers. Compared with other insulation materials, they are highly competitive. The air trapped within the honeycomb like structure developing passive insulation characteristics of foam in addition to polyurethanes' heat absorption capacity. They are also chlorofluorocarbon free and recyclable [13]. The attempt of applying PCMs in polyurethane foams to improve their thermal performance was developed in 1990s; the foams containing PCMs can improve the heat-insulating ability [14, 15]. According to different phase change temperatures of PCMs, the polyurethane foams can gain various applications, such as building energy conservation, energy saving technology for crude oil pipeline transportation. However, due to the chemical constitution of PU and paraffin, the composites are easily flammable whereas a decrease in the flammability becomes very important.

The fabrication of paraffin/polyurethane foams composite was presented in details. The effects of thermal properties and flame retardant properties of paraffin/polyurethane foams composite were investigated.

II. EXPERIMENTAL

A. Materials

Polyurethane foam mixed materials (stuff A: mixture of polyether polyol, foaming agent and so on. Stuff B: isocyanate) were purchased from Yantai Wanhua Co. Ltd., Shandong Province, China. The producer proposed weight ratio: stuff A:stuff B = 100:50, stuff temperature: 20-25℃, mold temperature: 55℃. The nano structured calcium carbonate (nano-CC) and red phosphorus (RP) were supplied by Jiangxi Huaming Co. Ltd., Jiangxi Province, China. Paraffin was made in FRIPP with the paraffin melting point 80-86℃, melting latent heat of 174.4kJ/kg.

B. Fabrication of Paraffin/Polyurethane Foams Composite with Flame Retardant

The predetermined masses of stuff A, paraffin and flame retardant were added in a beaker and mixed vigorously with strong stirring for 30s to obtain a formulated mixture. The predetermined masses of stuff B were then added into the same beaker with strong stirring for 60s. The resulted mixture was left undisturbed for about 5 min allowing the formation and growth of the foam. Then it was moved and kept in an oven at 50℃. Four kinds of paraffin/polyurethane foams composite were obtained, denoted PCM-1, PCM-2, PCM-3, and PCM-4. The compositions of paraffin, PU, and flame retardant in the composites are listed in Table Ⅰ.

TABLE Ⅰ THE COMPOSITIONS OF PARAFFIN, PU AND FLAME RETARDANT IN THE COMPOSITES

Samples	Compositions (in mass portions)
PCM-1	50g PU
PCM-2	50g PU + 10g Paraffin
PCM-3	50g PU + 10g Paraffin + 12g nano-CC
PCM-4	50g PU + 10g Paraffin + 12g nano-CC + 3g RP

C. *Characterization of Paraffin/Polyurethane Foams Composite with Flame Retardant*

The thermal properties of composites was obtained by using a differential scanning calorimeter (STA 449C Netzsch) at 5℃ /min under a constant stream of nitrogen at a flow rate of 20 ml/min. The structural analysis of composites was carried out using a FT-IR spectrometer. The FT-IR Spectra were recorded on a Nicolet 6700 from 500 to 4000 cm-1 with a resolution of 2 cm-1 using KBr pellets. Microstructures of the PU and composites were observed by using a SEM (Jeol 7500F, Japan) at room temperature. The flame retardant properties of composites was determined by limited oxygen index tester (JF-3, Jiangning Analysis Instrument Factory, China).

III. RESULTS AND DISCUSSION

A. *FT-IR Analysis of Paraffin/Polyurethane Foams Composite*

FT-IR spectra of the synthesized foams, namely PCM-1, PCM-2 and paraffin are presented in Fig. 1. The spectrum of PCM-1 presents all the distinctive bands of the polyurethane foams. The spectra of experimental groups are compared with that of PCM-1 and paraffin. The band of –OH stretching vibration at 3435-3352 cm-1 is associated with the free H2O, -OH groups of non-bonded polyol or -OH groups within the foams structure. Peaks related to –CN and –C=O at 2271 and 1708 cm-1 observed in the spectrum of PCM-1 disappear in the spectrum of PCM-2. This indicates incompleteness of PU chain arising from the addition of a secondary material into the structure. The intensity increases in peaks for –CH2 at 2955.9 and 2917.8 cm-1 of PCM-2 is associated with capturing paraffin.

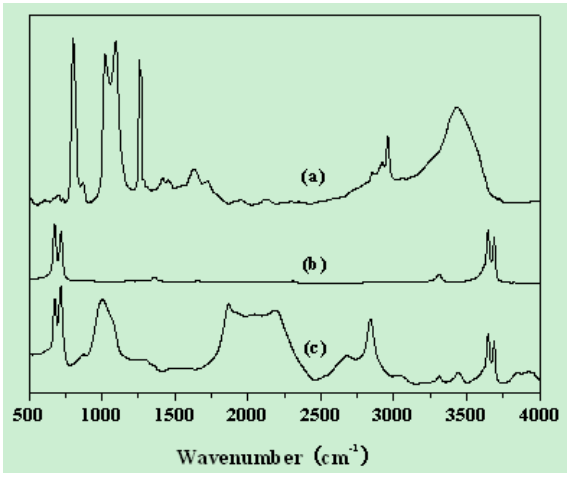

Fig. 1 FT-IR spectra of (a) PCM-1, (b) paraffin and (c) PCM-2

These characterized peaks are the evidence of a successful paraffin trapping in PU foams [16, 17]. It is meanwhile found that there is no shift in the absorption peaks of composites when compared with the spectra of paraffin. This result indicates that there is no chemical interaction between the functional groups of paraffin and PU.

B. *SEM Photos of Paraffin/Polyurethane Foams Composite*

SEM photos of PU foams and composites are shown in Fig. 2. Fig.2 (b) clearly illustrates some paraffin micelles distributing in PU foams. The excellent honeycomb structure obtained during foam formation made considerable amount of still air trapping possible, and effectively prevented the leakage possibility of paraffin [18,19].

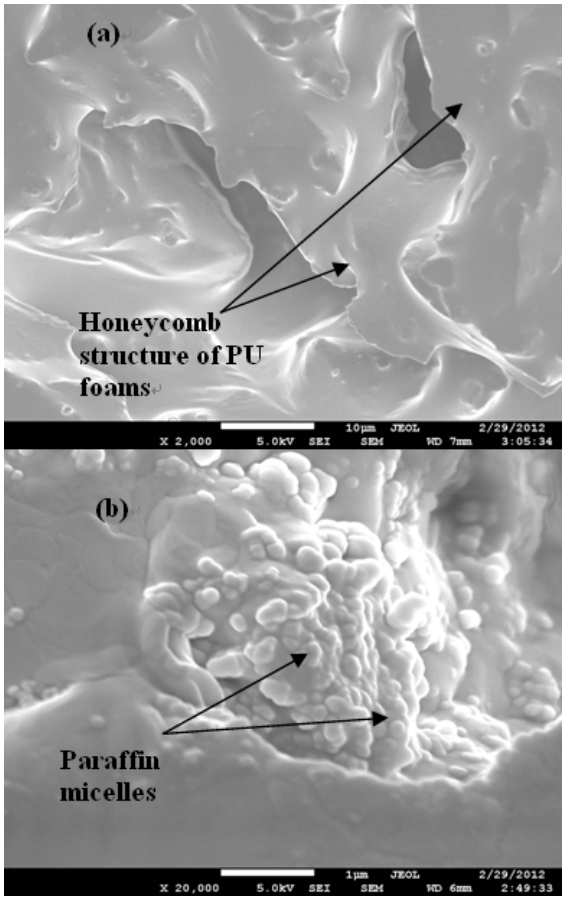

Fig. 2 SEM photos of (a) PU foams and (b) PCM-2

C. *The Thermal Properties of Paraffin/Polyurethane Foams Composite*

Fig. 3 illustrates DSC curves of PU foams with paraffin and flame retardant. Compared with the pure PU foams, paraffin/PU foams composite has endothermic peak in the process of heating in the point of 80.3℃, melting latent heat of 25.8kJ/kg. As shown in Table Ⅱ, flame retardant has no significant influence to the latent heat. After the addition of paraffin with different melting temperatures, different paraffin/PU foams composite with various phase change temperatures can be gained.

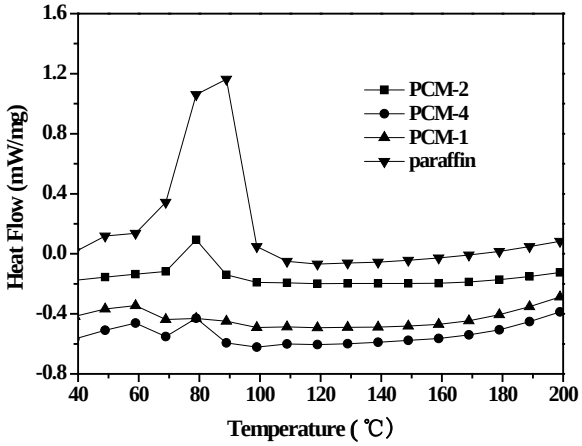

Fig. 3 The melting DSC curves of paraffin and PCMs

TABLE Ⅱ DSC DATA OF THE PARAFFIN AND PCMS

Sample	Solid-liquid melting	
	Temperature (℃)	Latent heat (kJ/kg)
paraffin	86.4	174.4
PCM-1	—	—
PCM-2	80.3	25.8
PCM-4	79.6	24.9

D. Flame Retardant Properties of Paraffin/ Polyurethane Foams Composite

The calculated LOI values of the prepared composites are presented in Table Ⅲ. Table Ⅲ shows that the LOI of the pure PU foams is only 16%. It is obvious that the addition of the flame retardant system into PU could improve the LOI value effectively and therefore promote the fire resistance.

TABLE 3 LOI VALUES OF COMPOSITES WITH AND WITHOUT THE FLAME RETARDANT SYSTEM

Sample	Compositions of flame retardant	LOI (%)
PCM-1	—	16
PCM-2	—	15
PCM-3	nano-CC	24
PCM-4	nano-CC + RP	27

The enhanced fire resistance of the flame retardant composites could be explained by the fire suppression mechanism of nano-CC and RP. The thermal decomposition of CC is an endothermic process, which can release CO2 to decrease temperature and dilute oxygen and flammable gases concentrated near the flame[20]. The decomposition product CaO is a fine flame material used as a retardant. The incorporation of RP into composites also improves the thermo-oxidative stability [21]. In a word, nano-CC and RP give a synergetic flame retarding effect to the composites.

IV. CONCLUSIONS

The preparation and properties of paraffin/PU foams composite with flame retardant are reported. Paraffin was used as PCM for thermal energy storage, and PU foams acted as the supporting material for improving the thermal stability of the composites. Nano-CC and RP were added in the composites in order to decrease the flammability of the composites. Paraffin was well dispersed in the honeycomb structure of the PU foams by capillary and surface tension forces, and the leakage of melted paraffin from the composites can be prevented even when it was heated above the melting temperature of the paraffin. As the mass percentage of paraffin in the composites was 16.7%, the composites melt at 80.3℃ with a latent heat of 25.8kJ/kg. The addition of nano-CC and RP in the composites improved the thermal stability and increased the LOI values from 16% to 27%.

ACKNOWLEDGEMENTS

The authors thank the China Petroleum & Chemical Corporation Foundation (Grant no. 031109) for financial support of this research. The authors also wish to thank reviewers for kindly giving revising suggestions.

REFERENCES

[1] K. Kaygusuz, T. Ayhan, “Exergy analysis of solar-assisted heat-pump systems for domestic heating”, Energy, 18,1077-1085, 1993.

[2] M.N. Roxas-Dimaano, T. Watanabe, “The capric and lauric acid mixture with chemical additives as latent heat storage materials for cooling application”, Energy, 27, 869-888, 2002.

[3] H. Benli, A. Durmus, “Performance analysis of a latent heat storage system with phase change material for new designed solar collectors in greenhouse heating”, Solar Energy, 83, 2109-2119, 2009.

[4] B. Zalba, J. M. Marin, L.F. Cabeza, H. Mehling, “Review on thermal energy storage with phase change materials”, heat transfer analysis and applications, Applied Thermal Engineering, 23, 251-283, 2003

[5] M. Kenisarin, K. Mahkamov, “Solar energy storage using phase change materials”, Renewable and Sustainable Energy Reviews, 11, 1913-1965, 2007.

[6] F. Agyenim, N. Hewitt, P. Eames, M. Smyth, “A review of materials, heat transfer and phase change problem formulation for latent heat thermal energy storage systems (LHTESS)”, Renewable and Sustainable Energy Reviews, 14, 615-628, 2010.

[7] A. Shukla, D. Buddhi, R.L. Sawhney, “Solar water heaters with phase change material thermal energy storage medium: a review”, Renewable and Sustainable Energy Reviews, 13, 2119-2125, 2009.

[8] A. Koca, H.F. Oztop, T. Koyun, Y. Varol, “Energy and exergy analysis of a latent heat storage system with phase change material for a solar collector”, Renewable Energy, 33, 567-574, 2008.

[9] W. Saman, F. Bruno, E. Halawa, “Thermal performance of PCM thermal storage unit for a roof integrated solar heating system”, Solar Energy, 78, 341-349, 2005.

[10] A. Pasupathy, R. Velraj, “Effect of double layer phase change material in building roof for year round thermal management”, Energy Building, 40, 193-203, 2008.

[11] V.V. Tyagi, D. Buddhi, “PCM thermal storage in buildings: a state of art”, Renewable and Sustainable Energy Reviews, 11, 1146-1166, 2007.

[12] A. Pasupathy, L. Athanasius, R. Velraj, R.V. Seeniraj, “Experimental investigation and numerical simulation analysis on the thermal performance of a building roof incorporating phase change material (PCM) for thermal management”, Applied Thermal Engineering, 28, 556-565, 2008.

[13] A. Demharter, “Polyurethane rigid foam: a proven thermal insulating material”, Cryogenics, 38, 113-117, 1998.

[14] Y.G. Bryant, D.P. Colvin, “Moldable foam insole with reversible enhanced thermal storage properties”, US Patent 5,499,460, 1996.

[15] R.L. Everitt, P.R. Harrison, R.V. Onufrak, “Energy absorbing, water blown, rigid polyurethane foam”, US Patent 6,028,122, 2000.

[16] R. Zhang, H. Xu, Y. Zhang, “Preparation, physical property and thermal physical property of phase change microcapsule slurry and phase change emulsion”, Solar Energy Materials & Solar Cells, 80, 405-416, 2003.

[17] K. Choi, G. Cho, P. Kim, C. Cho, “Thermal storage/release and mechanical properties of phase change materials on polyester fabrics”, Textile Research Journal, 74, 292-297, 2004.

[18] N. Sarier, E. Onder, “Thermal characteristics of polyurethane foams incorporated with phase change materials”, Thermochimica Acta, 454, 90-98, 2007.

[19] G.Y. Fang, H. Li, Z. Chen, X. Liu, “Preparation and properties of palmitic acid/SiO_2 composites with flame retardant as thermal energy storage materials”, Solar Energy Materials & Solar Cells, 95, 1875-1881, 2011.

[20] P.A. Larcey, J.P. Redfern, G.M. Bell, “Study on magnesium hydroxide in polypropylene using simultaneous TG-DSC”, Fire and Materials, 19, 283-285, 1995.

[21] Z.Z. Wang, G.S. Wu, Y. Hu, Y. Ding, K.L. Hu, W.C. Fan, “Thermal degradation of magnesium hydroxide and red phosphorus flame retardant polyethylene composites”, Polymer Degradation and Stability, 77, 427-434, 2002.

Liang Zhao (China, 1980-) majored in catalytic materials and gained a doctor degree of industrial catalysis in Dalian University of Technology at 2010, which was in Dalian city, Liaoning province, China.
He is working for Fushun Research Institute of Petroleum and Petrochemicals of SINOPEC since July 2010, which was in Fushun city, Liaoning province, China. And also, he is majoring in thermal energy storage, the published articles were as follows:

［1］Liang Zhao, Hongbo Wang, Min Liu, et al. "Shape-selective methylation of 2-methylnaphthalene with methanol over hydrothermal treated HZSM-5 zeolite catalysts", Chem. Eng. Sci., 63(21): 5298-5303(2008).
［2］ Liang Zhao, Xinwen Guo, Min Liu, et al. "Methylation of 2-methylnaphthalene with methanol over NH_4F and Pt modified HZSM-5 cataltsts", Chin. J. of Chem. Eng., 18(5):742-749(2010).
［3］Liang Zhao, Ruiying Ma, Xianglan Meng, et al. "Characterization and preparation of paraffin/modified inorganic porous materials composites as building energy storage materials', Adv. Mater. Res. 450-451:1419-1424(2012).

Gang Wang (China, 1968-) majored in petroleum refining engineering and gained a doctor degree of physical chemistry in Dalian Institute of Chemical Physics, Chinese Academy of Science at 2008, which was in Dalian city, Liaoning province, China.
He is working for Fushun Research Institute of Petroleum and Petrochemicals of SINOPEC, which was in Fushun city, Liaoning province, China. Also, he is a professor and majors in petroleum refining and thermal energy storage now.

Xiangchen Fang (China, 1960-) majored in petroleum refining engineering. He is working for Fushun Research Institute of Petroleum and Petrochemicals of SINOPEC, which was in Fushun city, Liaoning province, China. Also, he is a professor and majors in petroleum refining and thermal energy storage now.

Jianfeng Sun (China) majored in thermal energy storage. He is working for Fushun Research Institute of Petroleum and Petrochemicals of SINOPEC, which was in Fushun city, Liaoning province, China. Also, he is a senior engineer and majors in thermal energy storage now.

Chunyan Yang (China) majored in thermal energy storage. She is working for Fushun Research Institute of Petroleum and Petrochemicals of SINOPEC, which was in Fushun city, Liaoning province, China. Also, she is a engineer and majors in thermal energy storage now.

Stability, Oscillatory Modes, Bifurcations, and Chaotic Behavior of Complex Systems with Phase Control

Valerie P. Ponomarenko[1], Nikolay I. Zaytsev[2]

[1, 2]Research Institute of Applied Mathematics and Cybernetics,

Nizhegorodsky State University After N.I. Lobachevski, Nizhni Novgorod, Russia

[1]povp@uic.nnov.ru; [2]nikozay@yandex.ru

***Abstract*-This paper deals with the problem of nonlinear dynamics of complex system with phase control combining phase-locked loop and automatic gain control loop. The behavior of the examined system is described by nonlinear two- and four-dimensional sets of differential equations with periodical nonlinearities. Stability of synchronous mode, bifurcations determining boundaries of domain with quality different behavior of the considered system, and oscillatory modes arising in domain where synchronous mode is unstable are studied. Results are presented using two-parameter bifurcation diagrams, phase portraits of attractors, time realizations of oscillations, and Poincare maps.**

Keywords-Systems with Phase and Gain Control; Nonlinear Dynamics; Stability; Bifurcation; Transitions to Chaos

I. INTRODUCTION

At present, the systems with phase control are widely used. As known [Shakhgil'dyan and Lyakhovkin, 1972; Lindsey, 1972], such systems are traditionally intended to provide for and maintain the synchronous state, when the phase difference of reference and controlled signals becomes constant or, equivalently, the frequency difference of these signals is equal to zero. The systems may be also operating in non-synchronous modes with variable phase and frequency errors. The use of such modes opens wide possibilities for some nontraditional engineering and technological applications of phase control systems (generation of complex periodic and chaotic signals, data transmission and processing, etc. [Dmitriev and Shirokov, 2004; Dmitriev, Kletsov and Kuzmin, 2009]).

Among the studies of the systems with phase control, the study of dynamical modes, bifurcation, and transitions to chaotic behavior is extremely interesting. In this paper we investigate dynamical behavior of complex system with phase control combining phase-locked loop (PLL) and automatic gain control loop (AGCL). Different versions of such systems are of interest because they represent a circuit implementation of optimal algorithms for tracking estimation of variable parameters (phase angle $\vartheta(t)$ and amplitude $A(t)$ of receiving signal [Tikhonov and Kulman, 1975; Kulman, Zheronkina, 1969]).

Combined PLL and AGCL operate on the basic of synchronization between receiving (estimated) and reference signals. For that, PLL performs coincidence of the signals frequencies, and AGCL regulates amplification factor in the phase control loop so as to reduce the influence of input signal amplitude alternation on PLL operation. This paper is mainly devoted to investigation of the characteristics of the system's dynamical behavior that are due to application of first- and second-order low-frequency filters (LFFs) in control circuits, and to coupling via phase and gain control circuits.

II. THE SYSTEM MODELS UNDER CONSIDERATION

Equations describing the dynamics of the considered combined PLL and AGCL can be derived from the equations for estimates ϑ^* and A^* of input signal parameters ϑ and A obtained in [Tikhonov and Kulman, 1975; Kulman, Zheronkina, 1969]. These equations can be represented for mismatch $\varphi=\vartheta(t)-\vartheta^*(t)$ and amplitude ratio $x=A^*/A$ in the operator form ($p\equiv d/dt$) as follows [Ponomarenko, 1986]

$$\left.\begin{aligned} p\varphi/k_1 &= \gamma - K_1(p)\, x \sin\varphi, \\ x &= K_2(p)\left[G_0(x) + k_2\left(\cos\varphi + \alpha x \sin\varphi\right)\right]. \end{aligned}\right\} \quad (1)$$

In Equation (1), k_1 and k_2 are the amplification factors of control circuits; γ is the initial frequency mismatch; $G_0(x)$ depends on the gain control circuit structure and is expressed in the forms of $G_0(x)=\delta_0-k_2x$ and $G_0(x)=\sigma/x-k_2x$ [Tikhonov and Kulman, 1975], $\delta_0=A_0/A$ (A_0 is average input signal amplitude); σ is the gain control circuit parameter; $K_1(p)$ and $K_2(p)$ are the transfer functions of the LLFs in the PLL and AGCL control circuits; and α is the factor of coupling via control circuits. By complexity of Equations (1), we consider amplitude A as constant parameter having arbitrary positive values.

The types of LFFs are determined by the models using for description of dynamics of parameters ϑ and A. Consider the simplest first-order filters with transfer functions $K_1(p)=1$, $K_2(p)=1/(1+T_0p)$, where T_0 is a time constant. Equation (1) may be written in this case as

$$\left.\begin{aligned} d\varphi/d\tau &= \gamma - x\sin\varphi, \\ dx/d\tau &= \lambda\left(G(x) + \cos\varphi + \alpha x \sin\varphi\right), \end{aligned}\right\} \quad (2)$$

where $\tau=k_1t$ is dimensionless time, $G(x)$ is represented by functions: $G(x)=\delta-\beta x$ and $G(x)=\sigma/x-\beta x$, $\beta=1+1/k_2$, $\delta=\delta_0/k_2$, $\lambda=k_2/(T_0k_1)$. System (2) is a dynamical system determined on cylindrical phase surface $U_0=\{\varphi(\mathrm{mod}2\pi),x\}$.

Now consider the second-order filter in the PLL and first-order filter in the AGCL with transfer functions $K_1(p)=1/[1+(T_1+T_2)p+T_1T_2p^2]$, $K_2(p)=1/(1+T_0p)$, where T_1 and T_2 are the time constants. In this case, equation (1) are written as

$$\left.\begin{aligned} &d\varphi/d\tau = y, \quad dy/d\tau = z,\\ &\mu\, dz/d\tau = \gamma - x\sin\varphi - y - \varepsilon_1 z,\\ &\varepsilon_2\, dx/d\tau = G(x) + \cos\varphi + \alpha x\sin\varphi, \end{aligned}\right\} \qquad (3)$$

where $\varepsilon_1=(T_1+T_2)k_1$, $\varepsilon_2=T_0k_1/k_2$, $\mu=T_1T_2k_1^2$. System (3) is a dynamical system with four-dimensional cylindrical phase space $U=\{\varphi(\mathrm{mod}2\pi),y,z,x\}$.

Further, we will consider the Models (2) and (3) for the values of variable $x>0$. Since Models (2) and (3) are nonlinear, its nonlocal study encounters serious difficulties. Therefore, we apply qualitative-numerical methods of nonlinear dynamics and computer simulation.

III. DYNAMICAL STATES OF MODEL

At first, we discuss the problem of local stability of synchronous mode. The equilibrium states of System (2) situated in the half phase cylinder $x>0$ are determined from the equations

$$\gamma - x\sin\varphi = 0,\ G(x) + \cos\varphi + \alpha x\sin\varphi = 0. \qquad (4)$$

Consider Equations (4) as function $G(x)=\delta-\beta x$. In this case, from Equations (4) and the form of G(x), it follows that, for $0<\alpha<\beta$ and the values of $\gamma,\delta,\beta,\alpha\in Co$ where $Co=\{\gamma_1(\delta,\beta,\alpha)<\gamma<\gamma_2(\delta,\beta,\alpha)\}$, system (2) has two equilibrium states $A_1(\varphi_1,x_1)$ and $A_2(\varphi_2,x_2)$. The coordinates φ_1, x_1, φ_2, and x_2 are defined from Equation (4). For $\alpha>\beta$, the domain $Co=\{\gamma>\gamma_1(\delta,\beta,\alpha)\}$. If $\alpha=0$, the boundaries of domain C_0

$$\left.\begin{aligned} &\gamma_1(\delta,\beta) = -\frac{(\sqrt{\delta^2+8}+3\delta)\sqrt{16-(\sqrt{\delta^2+8}-\delta)^2}}{16\beta}\\ &\gamma_2(\delta,\beta) = -\gamma_1(\delta,\beta). \end{aligned}\right\} \qquad (5)$$

Bifurcation values $\gamma=\gamma_1$ and $\gamma=\gamma_2$ corresponding to merging of equilibrium states $A_1(\varphi_1,x_1)$, and $A_2(\varphi_2,x_2)$ are defined from equality

$$\gamma_i(\delta,\beta,\alpha)=\sin\varphi_{m2}(\delta+\cos\varphi_{m2})/(\beta-\alpha\sin\varphi_{m2}),\quad i=1,2. \qquad (6)$$

In Equality (6) $\varphi m2$ is the solution of the equation

$$\beta\cos\varphi(\delta+\cos\varphi)-\sin^3\varphi(\beta-\alpha\sin\varphi)=0. \qquad (7)$$

The values of $\varphi m2$ are satisfied following conditions: $-\pi/2<\varphi m1<0$, $0<\varphi m2<\pi/2$. Fig. 1 shows qualitative disposition of bifurcation curves γ_1 and γ_2, and domain Co on the (γ,δ) plane for $0<\alpha<\beta$ (Fig. 1a) and $\alpha>\beta$ (Fig. 1b).

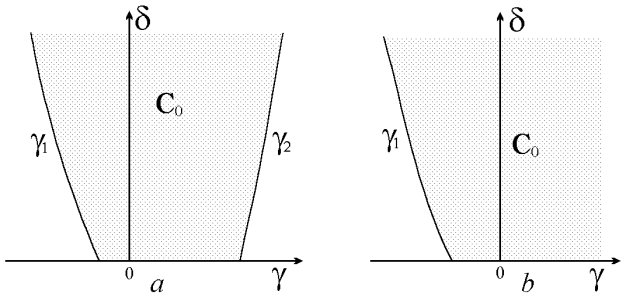

Fig. 1 Disposition of the domain C_0: *a* – $0<\alpha<\beta$, *b* – $\alpha>\beta$

Now consider Equations (4), if function $G(x)=\sigma/x-\beta x$. From (4) and the form of G(x), it follows that, for $0<\alpha<\beta$ and $\gamma,\delta,\beta,\alpha\in D_0$, where $D_0=\{\sigma>\max(\sigma-(\gamma,\beta,\alpha),0,\ \sigma^+(\gamma,\beta,\alpha))\}$, System (2) has also two equilibrium states $A1(\varphi_1,x_1)$ and $A1(\varphi_2,x_2)$. For $\alpha>\beta$, the domain is $D_0=\{\sigma>\max(\sigma-(\gamma,\beta,\alpha),0)\}$. If parameter $\alpha=0$, $\sigma^+(\gamma,\beta,\alpha)=\sigma-(-\gamma,\beta,\alpha)$. Bifurcation values $\sigma=\sigma-$ and $\sigma=\sigma^+$ corresponding to merging of equilibrium states $A_1(\varphi_1,x_1)$ and $A_2(\varphi_2,x_2)$ are defined by

$$\left.\begin{aligned} \sigma^+ &= \frac{\gamma^2(\beta-\alpha\sin\varphi_m^+)-\gamma\sin\varphi_m^+\cos\varphi_m^+}{\sin^2\varphi_m^+},\\ \sigma^- &= \frac{\gamma^2(\beta-\alpha\sin\varphi_m^-)-\gamma\sin\varphi_m^-\cos\varphi_m^-}{\sin^2\varphi_m^-}. \end{aligned}\right\} \qquad (8)$$

In (8) φ_m^+ and φ_m^- ($\varphi_m^+\in(0,\pi/2)$, $\varphi_m^-\in(-\pi/2,0)$) are the solutions of the equation

$$\gamma\,(2\beta-\alpha\sin\varphi)\cos\varphi-\sin\varphi=0. \qquad (9)$$

Disposition of bifurcation curves $\sigma=\sigma-$ and $\sigma=\sigma+$, and domain D_0 on the (γ,σ) plane is qualitatively similar to disposition of curves $\gamma=\gamma_1$ and $\gamma=\gamma_2$ on the (γ,δ) plane given in Fig. 1.

The characteristic equation for system (2) is

$$\chi^2 + q\chi + r = 0. \qquad (10)$$

In (10), if function G(x) takes the form $G(x)=\delta-\beta x$, then

$$\left.\begin{aligned} q &= \lambda(\beta-\alpha\sin\varphi_{1,2}) + x_{1,2}\cos\varphi_{1,2},\\ r &= \lambda(x_{1,2}\cos\varphi_{1,2}(\beta-\alpha\sin\varphi_{1,2}) +\\ &\quad +(\alpha x_{1,2}\cos\varphi_{1,2}-\sin\varphi_{1,2})-\sin\varphi_{1,2}). \end{aligned}\right\} \qquad (11)$$

If function G(x) takes the form $G(x)=\sigma/x-\beta x$, then in Equation (10)

$$\left.\begin{aligned} q &= \lambda(\sigma/x_{1,2}^2+\beta-\alpha\sin\varphi_{1,2})+x_{1,2}\cos\varphi_{1,2},\\ r &= \lambda(x_{1,2}\cos\varphi_{1,2}(\sigma/x_{1,2}^2+\beta-\alpha\sin\varphi_{1,2})-\\ &\quad -\sin\varphi_{1,2}(\sin\varphi_{1,2}-\alpha x_{1,2}\cos\varphi_{1,2})). \end{aligned}\right\} \qquad (12)$$

By investigating the roots of the characteristic Equation (10), we find that the equilibrium state $A_1(\varphi_1,x_1)$ are stable, whereas the equilibrium state $A_2(\varphi_2,x_2)$ is unstable of saddle type.

The equilibrium state A_1 corresponds to synchronous mode of combined PPL and AGCL. If this mode is realized in this system, then the system can carry out tracking of estimated input signal's parameters. The parameter region where such mode exists is limited by the values of parameters γ, δ, β, α, and σ those belong to domains C_0 and D_0. Values φ_1 and x_1 characterize the accuracy with which the parameters of input signal are estimated.

Further, we consider nonlocal dynamic processes evolving in Model (2) when parameters γ, δ, and σ vary and remaining parameters are fixed. The results of qualitative-numerical investigation of Model (2) for $G(x)=\delta-\beta x$ and for $G(x)=\sigma/x-\beta x$ reveal qualitatively similar dynamical states, bifurcation, parametrical portraits on the (γ,δ) plane and (γ,σ) plane, and corresponding phase portraits. Fig. 2 shows qualitative disposition of bifurcation curves on the (γ,δ) plane within the domain Co obtained for System (2), if function G(x) takes the form $G(x)=\delta-\beta x$ and $0<\alpha<\beta$.

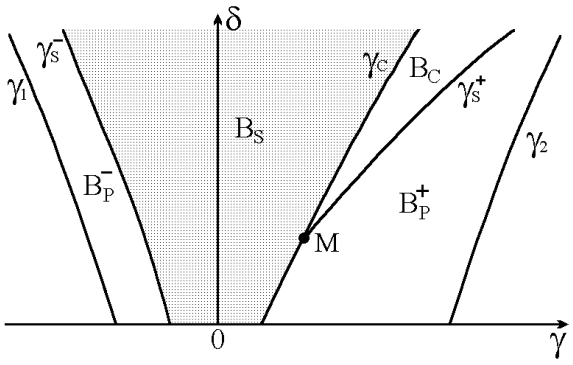

Fig. 2 Bifurcation curve and domains

of dynamical modes

In Fig. 2 lines γ_s^- and γ_s^+ correspond to saddle A_2 separatrix S_1 and S_2 loop Π0 of rotatory type that encompasses the phase cylinder U0. By investigating of saddle value:

$$\sigma_s = -x_2(\gamma,\delta,\beta,\alpha)\cos\varphi_2(\gamma,\delta,\beta,\alpha) - \lambda\beta + \\ + \mu\alpha\sin\varphi_2(\gamma,\delta,\beta,\alpha), \qquad (13)$$

we find that the loop Π0, that arises at $\gamma=\gamma_s^-$, is stable (saddle value σs<0), whereas the loop Π0, that forms at $\gamma=\gamma_s^+$, is stable at the part of the curve γ_s^+ below the point M (where σs<0) and unstable at the part of the curve γ_s^+ above the point M (where σs>0). The point M corresponds to δ=δs(γ, β, α, λ), that defined from the equation σs(γ,δ,β,α,λ)=0.

Therefore, upon passing throw the curve γ_s^-, if γ is decreased, a stable rotatory type (2π-periodic in φ) limit cycle L0 appears in the half phase cylinder x>0. When, as the result of γ increasing, the System (2) crosses line γ_s^+ and δ<δs, a stable rotatory type limit cycle L0 also appears in the half phase cylinder x>0. Upon passing throw the curve γ_s^+, as γ is decreased and δ>δs, an unstable rotatory type limit cycle Γ0 appears in the half phase cylinder x>0.

Line γc starting from the point M corresponds to double rotatory type limit cycle in the half phase cylinder x>0. If, as the result of increasing γ, line γc is crossed, a stable rotational type limit cycle L0 and an unstable rotatory type limit cycle Γ0 are born in the half phase cylinder x>0. Upon passing through the line γc, as γ is decreased, limit cycles L0 and Γ0 merge and disappear.

Limit cycle L0 is associated with the asynchronous mode of the combined PLL and AGCL such that phase error φ rotates and amplitude ratio x periodically oscillate about certain mean value.

Bifurcation curves γ_1, γ_s^-, γ_s^+, γc, and γ2 given at Fig. 2 identify various parameter domains possessing qualitatively different dynamics of the Model (2). Fig. 3 shows the phase portraits of the System (2) for dynamic mode domains represented in Fig. 2. For the parameters from domain $B_S=\{\gamma_s^- < \gamma < \min(\gamma_s^+, \gamma c)\}$ there are no limit cycles and equilibrium state A_1 of System (2) is globally asymptotically stable in the half phase cylinder x>0. The phase trajectories of System (2) converge to A_1 independently of initial state of the system (Fig.3a). Therefore, when the values of the system parameters belong to domain Bs, the combined PLL and AGCL is in synchronous mode irrespective of the initial conditions.

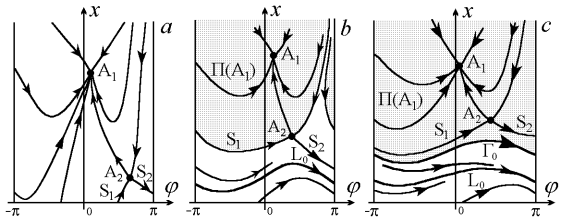

Fig. 3 Phase portraits of model (2)

For the parameters from domains $B_p^- = \{\gamma_1 < \gamma < \gamma_s^-\}$ and $B_p^+ = \{\gamma_s^+ < \gamma < \gamma 2\}$ a stable equilibrium state A_1 and stable limit cycle L0 are simultaneously exist on the phase cylinder U0 (Fig. 3b). Depending on initial state, the trajectories of System (2) converge either to equilibrium state A_1 or to limit cycle L0. Therefore, depending on initial conditions, synchronous or asynchronous mode corresponding to these attractors on the phase cylinder U0 develops in the combined PLL and AGCL. The regions of attraction of equilibrium state A_1 and limit cycles L0 are bounded by of saddle A_2 separatrix on the phase cylinder U0. For the parameters from domain $Bc=\{\gamma c < \gamma < \gamma_s^+\}$ there are equilibrium state A_1 and limit cycles L0 and Γ0 on the phase cylinder U0 (Fig. 3c). The region Π(A1) of attraction of equilibrium state A_1 is bounded by unstable limit cycle Γ0. Therefore, if the initial conditions belong to domain located above limit cycle Γ0, then the synchronous mode is realized in combined PLL and AGCL.

From the results obtained in framework of Model (2) we infer that, coupling via feedback signals in combined PLL and AGCL with the first-order filters make possible the appearance of asynchronous mode of rotational limit cycle, which is not possible in partial PLL and AGCL.

IV. PECULIARITIES OF MODEL (3) DYNAMICAL BEHAVIOR

If second-order LFF is used in the PLL, the dynamics of combined PLL and AGCL becomes drastically more complex. In addition to the synchronous mode and the periodic asynchronous mode, complex-periodic and chaotic asynchronous modes appear. Apart from this, the synchronous mode may lose stability and a transition to a periodic quasi-synchronous mode characterized by an oscillatory-type limit cycle may occur, the quasi-synchronous mode may become chaotic. Besides, the system may exhibits quasi-synchronous and asynchronous modes of quasi-periodic types corresponding to oscillatory and rotational two-dimension tori in the phase space.

First, let us analyze the stability of the combined PLL and AGCL synchronous mode. System (3) with parameters $\gamma,\delta,\beta,\alpha \in Co$ and $\gamma,\sigma,\beta,\alpha \in D_0$ has two equilibrium states $A_1(\varphi_1,0,0,x_1)$ and $A_2(\varphi_2,0,0,x_2)$ located within the range x>0 of phase space U; coordinates $\varphi_1, x_1, \varphi_2$, and x_2 are determined from (4). Equilibrium state A_1 may be either stable or unstable, while equilibrium state A_2 is unstable of saddle type.

The conditions under which equilibrium state A_1 is stable are determined by the roots of characteristic

Equation:

$$\chi^4 + a_1\chi^3 + a_2\chi^2 + a_3\chi + a_4 = 0, \qquad (14)$$

where

$$\left.\begin{aligned} a_1 &= \varepsilon_1/\mu - (G'(x_n) + \alpha\sin\varphi_n)/\varepsilon_2, \\ a_2 &= (1 - \varepsilon_1(G'(x_n) + \alpha\sin\varphi_n)/\varepsilon_2)/\mu, \\ a_3 &= (x_n\cos\varphi_n - (G'(x_n) + \alpha\sin\varphi_n)/\varepsilon_2))/\mu, \\ a_4 &= -(\sin^2\varphi_n + x_n G'(x_n)\cos\varphi_n)/(\mu\varepsilon_2). \end{aligned}\right\} \qquad (15)$$

Applying the Routh-Hurwits criterion to the Equation (14), we obtained that equilibrium state A_1 is stable for the values of parameters such that the following inequalities hold:

$$a_1,a_2,a_3,a_4>0,\ a_1a_2-a_3>0,\ a_3(a_1a_2-a_3)-a_1^2a_4>0. \qquad (16)$$

If Condition (16) are satisfied, the combined PLL and AGCL described by Model (3) have a synchronous mode corresponding to equilibrium state $A_1(\varphi_1,0,0,x_1)$.

The domain of parameters Cs0 where Conditions (16) are satisfied corresponds to the region where the synchronous mode persists. Figs. 4 and 5 show boundary of the domains Co and D_0 where the equilibrium states exist (curve γ_1) and boundary of domain Cs0 where equilibrium state A_1 is stable (curve γs), for $G(x)=\delta-\beta x$ (Fig. 4) and $G(x)=\sigma/x-\beta x$ (Fig. 5) correspondently.

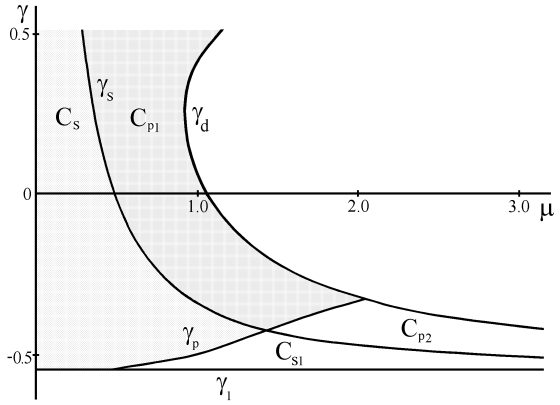

Fig. 4 Bifurcation diagram (μ,γ) for G(x)=δ−βx

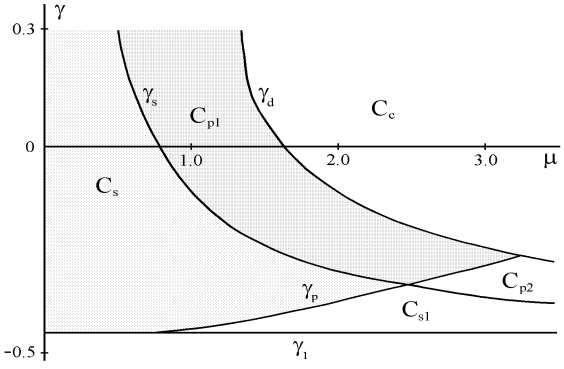

Fig. 5 Bifurcation diagram (μ,γ) for G(x)=σ/x−βx

The curves γ_1 and γs, and other bifurcation curves are plotted on plane (μ,γ) for the values of parameters α=2, β=1.1, ε_1=1, ε_2=2, δ=1.25, σ=0.5. The domain Cs0 is located between the lines γs and γ_1.

The domain Cs0 is divided by the curve γp into domains Cs: {max (γ_1,γp)<γ<γs} and Cs_1:{γ_1<γ<min(γp, γs)}. The curve γp corresponds to the bifurcation of saddle-focus A_2 separatrix loop rotatory type (Re$\chi_{1,2}$<0, Im$\chi_{1,2}\neq$0, χ_3<0, χ_4>0, where χ1,2,3,4 are the roots of the characteristic equation (14) for the equilibrium state A_2). For the parameters from domain C_s, the equilibrium state A_1 is only attractor in the phase space U. The trajectories in the phase space converge to A_1 independently of initial state of the system. Therefore, the domain C_s is a locking region of the combined PLL and AGCL. When the values of the Model (3) parameters belong to domain C_s, the system is in the synchronous mode irrespective of the initial conditions.

Now let us consider qualitative change of the system's behavior that occurs owing to variations in γ and μ during the exit from domain C_s. When, as a result of growing γ or μ, the system crosses boundary γs, Conditions (16) are violated and System (3) exhibits the Andronov-Hopf supercritical bifurcation. The latter is related to a solution to characteristic Equation (14) containing a pair of complex-conjugated roots with a positive real part. At the same time, oscillatory type limit cycle S1 such that phase difference φ varies within a limited range not exceeding 2π appears in phase space U. Cycle S1 corresponds to a quasi-synchronous mode in the combined PLL and AGCL where periodic oscillations of phase variables are observed around equilibrium state A_1 that has become unstable. Fig. 6a shows (φ,y)-projection of phase portrait and time waveform y(τ) corresponding to the mode of cycle S1 of model (3) for $G(x)=\delta-\beta x$.

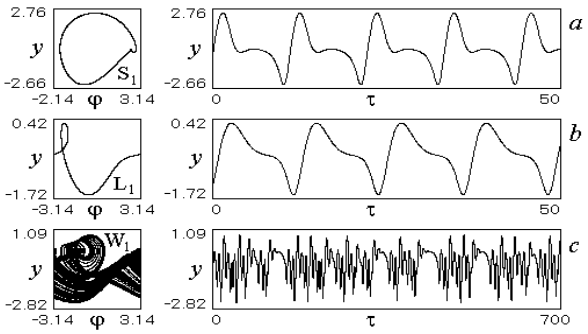

Fig. 6 Nonsynchronous modes of model (3) for $G(x)=\delta-\beta x$ and γ=0.86, μ=0.727 (a); γ=−0.54, μ=1.6 (b), 2.63 (c) (α=2, β=1.1, δ=1.25, ε_1=1, ε_2=2)

If, as a result of increasing μ or decreasing γ, the system crosses line γp (where the saddle value $\sigma p=\chi_4+\mathrm{Re}\chi m<0$, m=1,2,3) a stable rotatory type limit cycle L1 appears in the phase space U. In the mode of limit cycle L1 phase difference φ rotates and variables y,z, and x periodically oscillate about certain mean values.

Upon changing of parameters γ and μ within the domain C_{s1} (see Figs. 4, 5) limit cycle L1 may disappear in the result of saddle-node bifurcation. After this bifurcation, the system undergoes a transition to the mode of rotatory chaotic attractor W_1 via intermittence. Figs.6b, 6c show examples of (φ,y)-projections of phase portraits and dependences y(τ) corresponding to the modes of attractors L_1 and W_1 of Model (3) for $G(x)=\delta-\beta x$. Modeling of System (3) indicates that complex multi turn-over rotatory type limit cycles exist in the phase space U when the system's parameters belong to domain C_{s1}. Therefore, in domain C_{s1}, combined PLL and AGCL have concurrent synchronous mode and asynchronous mode determined by stable equilibrium state and periodic or chaotic attractors of rotatory type. The initial conditions determine

which of these modes is realized in the system for parameters from the domain C_{s1}.

The quasi-synchronous mode of limit cycle S1 exists for the values of parameters belonging to domain Cp_0 restricted by the curves γs and γd (see Figs. 4, 5). Curve γd corresponds to the loss of stability of limit cycle S1 as the result of the period-doubling bifurcation. The domain Cp_0 is divided by bifurcation curve γp into domain Cp_1: {max(γs,γp)<γ<γd} and Cp_2: {γs<γ<min(γp, γd)}. For the parameter values from domain Cp_1, limit cycle S1 is globally stable. While for the parameters from domain Cp_2 -the Model (3) exhibits bistable behavior, the limit cycle S1 and periodic or chaotic modes of attractors of rotational type concurrently exist in the phase space U. Transitions to the chaotic mode are realized via period-doubling bifurcations of rotatory limit cycles and so via intermittence.

In domain C_c, located to the right of line γd, the Model (3) exhibits complex dynamical behavior. For parameters from the domain C_c quasi-synchronous and asynchronous modes of various complexities are realized in the combined PLL and AGCL.

Let us track the evolution of the mode of limit cycle S1 when parameter μ is increased. For this purpose, we use the results of numerical simulation of Model (3) for $G(x)=\sigma/x-\beta x$. The non-synchronous modes formed when parameter μ varies are illustrated by one-parameter bifurcation {μ,y} diagram of the Poincare mapping corresponding to σ=0.5, β=1.1, α=2, ε_1=1, ε_2=2, γ=0.1, and μ∈(1.4;2.82) (Fig.7), (φ,y) projections of the attractors' phase portraits, and fragments of dependences y(τ) (Fig.8).

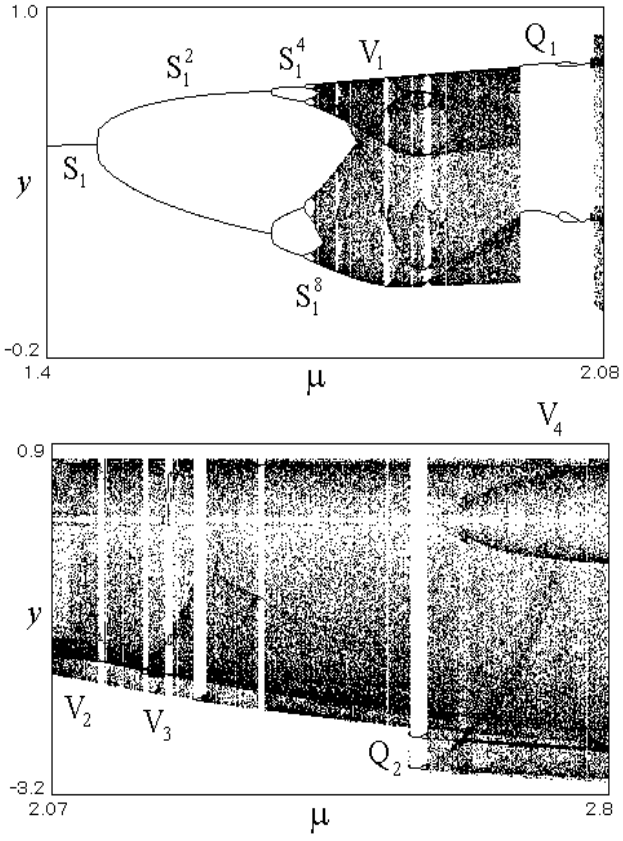

Fig. 7 Diagram showing evolution of quasi-synchronous mode of limit cycle S_1 during variation of μ for $G(x)=\sigma/x-\beta x$

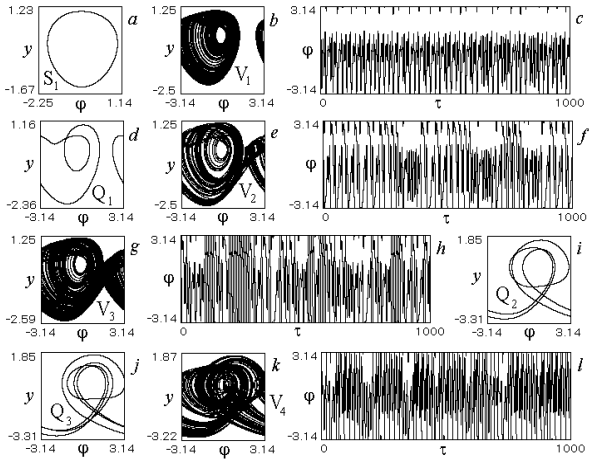

Fig. 8 Projections of phase portraits and fragments of time-realizations of oscillations corresponding to attractors of model (3) for $G(x)=\sigma/x-\beta x$, μ=1.4 (a); 1.95 (b,c); 2.0 (d);

2.07 (e,f); 2.21 (g,h); 2.55 (i); 2.62 (j); 2.82 (k,l)

(σ=0.5, β=1.1, α=2, ε_1=1, ε_2=2, γ=0.1)

The quasi-synchronous mode of limit cycle S1 is the system's initial state. When μ increases, cycle S1 exhibits period-doubling bifurcations, which finally end in a transition to the mode of oscillatory chaotic attractor V_1 (Figs. 8b, c). After that, the oscillations in the mode of attractor V_1 transform rigidly into the oscillations in the mode of oscillatory limit cycle Q_1 (Fig. 8d). When μ>2.07, the system switches from the mode of limit cycle Q_1 to the mode of chaotic attractor V_2 of oscillatory-rotatory type (Figs. 8e,f). Then, alternating chaotic and periodic asynchronous modes are observed; in the majority of the studied μ range, chaotic modes are realized. Examples of phase portraits and time realization y(τ) of chaotic and periodic modes are shown in Figs. 8g-8l.

Numerical simulation of Model (3) reveals that this model may demonstrate such interesting dynamical phenomena as formation of attracting two-dimensional tori of oscillatory and rotatory types in the phase space U. These tori appear as the result of loss of oscillatory or rotatory limit cycles stability when a pair of complex-conjugated cycles, multiplicators crosses a unit circle. The tori correspond to two-frequency non-synchronous modes of combined PLL and AGCL.

Fig. 9 illustrates the examples of the (φ,x)-projection of phase portraits, dependences x(τ), and (y, x)-projections of Poincare mapping T generated by the phase trajectories of Model (3) corresponding to $G(x)=\delta-\beta x$ and β=1.1, δ=1.25, γ=0.1, μ=5, ε_1=1.97, ε_2=150. The results represented in Fig. 9 characterize non-synchronous modes of the system formed when coupling parameter α varies. The quasi-synchronous mode of limit cycle S_2 (see Fig. 9a) is the system's starting state for α=1.6.

When α increases, the mode of oscillatory torus T1 (Fig. 9b) appears from limit cycle S_2. The phase portrait of mapping T (Fig. 9c) is characterized by the presence of stable closed invariant curve Γ_1. When 1.623<μ<1.92, the alternation of the mode of torus T1 and the modes of multi turn-over limit cycles of oscillatory type are observed. An example of nine-turn limit cycle S_3 is represented in Fig. 9d. Beginning with α=1.92, the distortion of the curve Γ_1 is observed. This phenomenon indicates gradual transformation the mode of torus T1 to the mode of oscillatory type chaotic attractor P_1 (Fig. 9e).

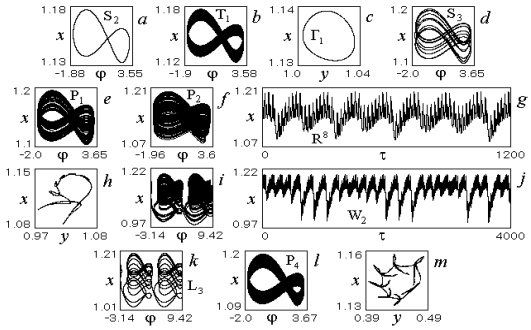

Fig. 9 Attractors of model (3) for G(x)=δ−βx and

α=1.6 (a); 1.65 (b,c); 1.9 (d); 1.946 (e); 2.08 (f,g,h);

2.097 (i,j); 2.35 (k); 2.436 (l,m)

(γ=0.1, μ=5, β=1.1, δ=1.25, ε1=1.97, ε2=150)

As α further increases, rigid transition of the system from the mode of chaotic attractor P_1 to the mode of oscillatory eight-turn limit cycle S_4 take place. With further increase of α the mode of cycle S_4 is transformed to the mode of chaotic attractor P_2 (Fig. 9f,g,h). Upon reaching the value α=2.088, rotatory phase trajectory scrolls in the attractor's P_2 structure are appeared. This phenomenon indicates transformation the mode of oscillatory attractor P_2 to the mode of oscillatory-rotatory chaotic attractor W_2 (Fig. 9i, j). A still increase of α leads to the alternation of the modes of complex limit cycles of oscillatory-rotatory types (Fig. 9k) and the modes of chaotic attractors (Fig. 9l, m) and following returning to the mode of periodic quasi-synchronous mode.

The existence of rotatory tori in phase space U is revealed in the model (3) for G(x)=δ−βx and β=1.1, δ=1.25, α=5, μ=5, ε_1=1, ε_2=150 when parameter γ is varied. Figure 10 displaying the examples of (φ,y)-projection of phase portraits, dependences y(τ), and (y,x)-projections of Poincare mapping Tφ of the plane φ=φ_0 into the plane φ=φ_0+2π produced by the trajectories of model (3) shows how mismatch γ affects the process of the asynchronous mode of limit cycle L_2 (Fig. 10a) transformation during a decrease in γ.

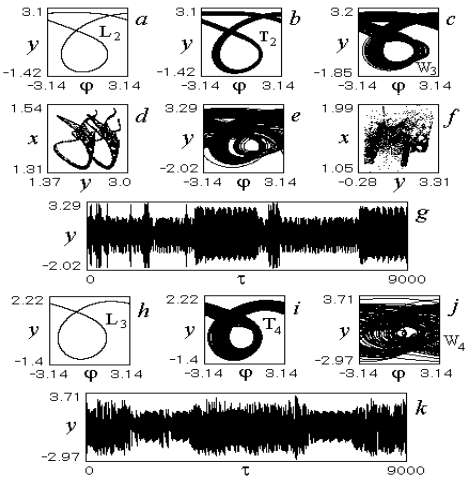

Fig. 10 Attractors of model (3) for G(x)=δ−βx and

γ=0.853 (a); 0.845 (b); 0.819 (c,d); 0.818 (e,f,g);

0.362 (h); 0.323 (i); 0.32 (j,k)

(α=5, μ=5, β=1.1, δ=1.25, ε_1=1.0, ε_2=150)

At first, the mode of limit cycle L_2 is transformed to the mode of rotatory torus T2 (Fig. 10b). Torus T2 corresponds to asynchronous two-frequency mode of the combined PLL and AGCL. Further, the following phenomena are observed in the system with decreasing γ: alternation of the mode of torus T2 and the modes of asynchronous modes of multi turn-over rotatory limit cycles; gradual transformation of torus T2 to chaotic attractor W3 (Fig. 10c, d); alternation of chaotic (Fig. 10e, f, g) and periodic modes, the latter of which is determined by two-, four-, and three-turn rotatory limit cycles; soft transformation of the mode of three-turn rotatory limit cycle to the mode of rotatory torus T3; distortion of the torus T3 and following transition to the chaotic mode. A still decrease of γ leads to transition of the system to the asynchronous mode of rotatory limit cycle L_3 (Fig. 10h) and following soft transformation of mode of cycle L_3 to the mode of rotatory torus T4 (Fig. 10i). When γ continues to decrease, the mode of torus T4 is transformed to the mode of rotatory chaotic attractor W_4 (Fig. 10j, k).

V. CONCLUSION

In this paper, we have investigated the dynamical modes, bifurcation, and transitions to the chaotic behavior in a combined PLL and AGCL with the first- and second-order filters in PLL and the first-order filter in AGCL. Using the dynamical models of considered systems, we found that the systems exhibit a rich variety of dynamical modes including synchronous mode, periodic quasi-synchronous mode caused by the loss of the synchronous mode stability, asynchronous modes of rotatory and oscillatory-rotatory limit cycles, quasi-periodic quasi-synchronous and asynchronous modes corresponding to oscillatory and rotatory 2D tori in the phase space, chaotic modes that formed via period-doubling bifurcations, via intermittence, as well as rigidly formed through saddle-node bifurcations of limit cycles, via destruction of tori. These phenomena, in our opinion, are of importance for both basic and applied research of nonlinear dynamics of complex systems with phase control. It allows describing and explaining the behavior of the system when the synchronous state is cut off as a result of the system parameters perturbation. The wide variety of chaotic modes offers considerable possibilities of forming various frequency- and amplitude-modulated signals at the output of the system. Control the characteristics of generated signals can be easily realized by means of system's parameters.

REFERENCES

[1] Shakhgil'dyan, V. V. and Lyakhovkin, A. A. (1972). Phase-Lock Systems. Svyaz', Moscow [in Russian].

[2] Lindsey W. (1972). Synchronization Systems in Communication and Control, Prentice-Hall, Englewood Cliffs, New Jersey.

[3] Dnitriev, A.S. and Shirokov, M.E. (2004). Choice of oscillator for direct chaotic communication system. Radiotekh. Electron. (Moscow), 49 (7), pp. 840-849. [in Russian].

[4] Dnitriev, A.S., Kletsov, A.V., and Kuzmin, K.V. (2009). Generation of ultra wideband phase chaos in decimeter range. Radiotekh. Electron. (Moscow), 54 (6), pp. 709-718. [in Russian].

[5] Tikhonov, V. I. and Kulman, N.K. (1975). Nonlinear filtering and quasi-coherent of signals reception. Sovetskoe Radio. Moscow [in Russian].

[6] Kulman, N.K. and Zheronkina, N.N. (1969). Optimum reception noise immunity of quasi-harmonic process with mutual correlated amplitude and phase. Radiotekh. Electron. (Moscow), 14 (11), pp. 2050-2054. [in Russian].

[7] Ponomarenko, V.P. (1986). On modes and capture range of phase locked loop with control gain circuit. Radiotekh. Electron. (Moscow), 31 (10), pp. 2023-2031. [in Russian].